Novel roles for *BicD* in pronuclear fusion and meiosis II progression via localization of the CHC/TACC/Msps complex to MII spindles

Paula Vazquez-Pianzola[1*], Dirk Beuchle[1], Gabriela Saro[1], Greco Hernández[2], Giovanna Maldonado[2], Dominique Brunßen[1], Peter Meister[1] and Beat Suter[1*].

[1] Institute of Cell Biology, University of Bern, 3012 Berne, Switzerland.

[2] Laboratory of Translation and Cancer, Unit of Biomedical Research on Cancer, Instituto Nacional de Cancerología (INCan), Mexico City, Mexico.

[*]Authors for correspondence: (beat.suter@izb.unibe.ch, paula.vazquez@izb.unibe.ch)

keywords: *Drosophila* meiosis, mitosis, spindle assembly, clathrin, Bicaudal-D, BicD, TACC, CH-TOG, microtubule transport, deGradFP.

short title: Novel role for *BicD* in meiotic spindle assembly

ABSTRACT

Vertebrate Clathrin heavy chain (Chc) plays a moonlighting function during mitosis. Chc forms a complex with TACC3 (Transforming Acidic Coiled Coil 3) and ch-TOG (colonic hepatic tumor overexpressed gene) at the spindle microtubules, forming inter microtubule bridges that stabilize the K-fibers. Since *Drosophila* Chc is a cargo of the dynein adaptor Bicaudal-D (BicD), we investigated whether BicD regulates Clathrin function at the spindle. We found that BicD localizes, like Chc, to centrosomes and spindles during mitosis and meiosis II, and that Chc interacts with *Drosophila* TACC (D-TACC). Using deGradFP to reduce the activity of BicD in mature eggs and very young embryos, we uncovered a novel function of BicD in meiosis II. The affected meiosis II products underwent abnormal rounds of additional replications and failed to carry out pronuclear fusion. Pointing to a mechanism, we found that the localization of Clathrin/D-TACC/Minispindles (Msps, homolog of ch-TOG) to the meiosis II spindles was impaired upon BicD knockdown. Furthermore, the meiotic products showed abnormal staining for PH3 and reduced recruitment of spindle assembly checkpoint (SAC) components. Altogether, our results support the notion that BicD performs a key activity in assembling the meiotic spindle apparatus. This function of BicD seems conserved in evolution because *C. elegans* embryos with reduced activities of these genes developed comparable phenotypes.

INTRODUCTION

Meiosis and mitosis are cell division mechanisms essential for the life and reproduction of eukaryotes. The spindle apparatus is the primary structure involved in the segregation of chromosomes during these processes. Consequently, aberrant spindle assembly during meiosis frequently leads to chromosome segregation problems and aneuploidy, which is the primary cause of infertility, pregnancy loss and mental congenital defects in humans. Additionally, mitotic errors leading to aneuploidy during early embryogenesis are mainly lethal. When such errors occur later in life, they lead to premature aging and tumorigenesis (Levine and Holland, 2018). The spindle apparatus comprises three classes of microtubules (MTs): astral MTs extending from the centrioles towards the cell cortex, interpolar MTs connecting the spindle poles (centrosomes), and kinetochore MTs. Kinetochore MTs bundle together into K-fibers (kinetochore fibers) connecting the spindle poles with the kinetochores in the centromere region of the chromosomes. They are most directly responsible for chromosome segregation.

Structurally, K-fibers are cross-linked MTs with electron-dense inter-MT bridges composed of motor proteins or non-motor microtubule-associated proteins (MAPs). Among these, clathrin was shown to be part of the mitotic spindles in mammalian and *Xenopus* cells

(Fu et al., 2010; Royle et al., 2005). This observation was surprising, as clathrin was best known for its central role in receptor-mediated endocytosis. Clathrin is composed of three Clathrin heavy chains (Chc) and three Clathrin light chains (Clc) shaped as a trimer scaffold protein (called triskelion) (Brodsky, 2012). On K-MTs, Clathrin was shown to play a non-canonical or moonlighting activity by stabilizing the spindle microtubules during mitosis (Royle, 2012). This function depends on clathrin trimerization and its interaction with Aurora A-phosphorylated Transforming Acidic Coiled-Coil protein 3 (TACC3) and the protein product of the colonic hepatic Tumor Overexpressed Gene (ch-TOG) (Booth et al., 2011; Fu et al., 2010; Lin et al., 2010; Royle and Lagnado, 2006; Royle et al., 2005). This heterotrimeric complex is recruited to the spindle microtubules and required to form inter microtubule bridges between K-fibers. The complex thereby stabilizes these fibers and promotes chromosome congression (Booth et al., 2011; Royle et al., 2005). This function explains why the lack of Chc results in cells with persistent activation of the spindle checkpoint (Royle et al., 2005).

The TACC3/Chc/ch-TOG complex also plays a role during meiosis. Clathrin was first reported to localize to the second metaphase spindle in unfertilized mouse eggs (Maro et al., 1985). ch-TOG and Chc localize to the meiosis I (MI) spindle in mouse oocytes (Lu et al., 2017). More recently, Aurora A-phosphorylated TACC3 together with one of the mammalian homologs of Chc (CHC17) were shown to control the formation of a new liquid-like spindle domain (LISD). These promote the assembly of acentrosomal mammalian oocyte spindles, and their disruption leads to severe spindle defects (So et al., 2019). In *Drosophila,* homologs of TACC (D-TACC) and ch-TOG (Mini spindles, Msps), are also enriched at the anastral poles of the MI spindles in stage 14 oocytes (Cullen and Ohkura, 2001).

We and others have found that Chc binds *Drosophila* Bicaudal-D (BicD) (Li et al., 2010; Vazquez-Pianzola et al., 2014). This interaction facilitates Chc transport, which is required for vesicle recycling at the neuromuscular junction, and for the assembly of the pole plasm during oogenesis. Encoded by a single gene, the *Drosophila* BicD protein is part of a family of evolutionarily conserved dynein adaptor proteins responsible for the transport of different cargoes along microtubules (Vazquez-Pianzola and Suter, 2012; Vazquez-Pianzola et al. 2016). The founding member of this protein family, *Drosophila* BicD, was identified as a protein essential during oogenesis and embryo development through its role in the intracellular transport of mRNAs which control polarity and cell fate (Bullock and Ish-Horowicz, 2001; Suter and Steward, 1991; Suter et al., 1989; Wharton and Struhl, 1989). This process is mediated by its binding to the RNA-binding protein Egalitarian (Egl) (Dienstbier et al., 2009; Mach and Lehmann, 1997). However, since then, BicD orthologs have been shown to control a diverse group of microtubule transport processes through binding to different

cargoes or adaptor proteins (Hoogenraad and Akhmanova, 2016; Vazquez-Pianzola and Suter, 2012).

Because BicD was shown to form complexes with both Chc and Dynein, both of which perform essential activities during mitosis, we set out to investigate possible *BicD* functions in spindle assembly during cell division processes. The syncytial *Drosophila* embryo´s fast and synchronous mitotic divisions provide a unique system to study the function of genes involved in cell cycle regulation. Thus, using fly embryos, we found that BicD localized, like Chc, to the mitotic spindles and centrosomes and that the interaction between Chc and TACC is conserved in *Drosophila*. Additionally, using a degradFP system, to reduce the levels of BicD::GFP after egg activation, we found that BicD plays an essential role during embryogenesis where it is needed for normal progression of meiosis II and pronuclear fusion. We found that BicD is needed to correctly localize D-TACC, Clc and Msps to the meiotic II spindles. It is also required for the normal metaphase arrest of polar bodies after meiosis II completion. Consequently, spindle assembly components (SAC) were not localized to meiotic products in embryos with reduced *BicD* activity, nor was chromatin phosphorylated on histone H3. This suggests that BicD, through its role in localizing the Clathrin/D-TACC/Msps complex, is needed to stabilize the meiotic II spindle K-fibers and required for the normal function of the meiosis II checkpoint. We further report that the function of these genes in pronuclear fusion is conserved all the way to the distant nematodes. *C. elegans tac-1* and *Chc* serve similar roles in the embryo as *Drosophila tacc* and *BicD*.

RESULTS

BicD and its cargo Clathrin localize to centrosomes and mitotic spindles during embryogenesis

Completion of female meiosis and the first mitotic cycles depend on the correct spindles formation in the developing embryo. Maternally expressed genes are involved in this process because the first zygotic transcription starts only in the 10th division cycle in the young embryo (De Renzis et al., 2007; Edgar and Schubiger, 1986). Maternal genes are also necessary for oocyte differentiation and gamete formation. Accordingly, inactivation of these genes leads either to maternal effect lethality or female sterility. Indeed, *BicD* loss-of-function mutants are female sterile because they do not produce oocytes (Ran et al., 1994). This is an obstacle for studying the role of *BicD* in the maternally controlled early mitotic divisions of the embryo. Our laboratory has developed the *BicD^{mom}* females, a method to overcome *BicD* mutant female sterility, and analyze the protein´s function in late oogenesis (Swan and Suter, 1996). Using this strategy, we observed that most of the embryos laid by *BicD^{mom}* females do not develop and arrest very early during embryogenesis (Supplementary Fig. S1A). This

suggests that *BicD* is also essential downstream of oocyte differentiation to complete meiosis and or progression through the early mitotic divisions.

To further understand whether *BicD* functions during mitosis, we analyzed its localization in methanol-fixed embryos using immunofluorescence. Methanol fixation dissolves the cytosolic pool of BicD, making insoluble pools of the protein more apparent. Surprisingly, BicD was detected on the centrosomes where it colocalized with centrosomin (Cnn), as well as on mitotic spindles (Fig. 1A). To exclude off-target recognition by the BicD antibody, we additionally analyzed embryos expressing BicD::GFP by immunofluorescence after staining them with anti-GFP. Both staining patterns were highly similar (Fig. 1B).

We previously reported that BicD interacts with the *Chc* messenger RNA and the Chc protein, and that it transports them inside the oocyte during oogenesis (Vazquez-Pianzola et al., 2014). Since Chc performs a moonlighting function at the mitotic spindles in vertebrates, we analyzed the expression of the Chc protein in *Drosophila* embryos using differently tagged Chc fusions that are functional (Vazquez-Pianzola et al., 2014). Chc was enriched apically in blastoderm embryos (Fig. 1C, Chc::V5 and Supplementary Fig. S1B, Myc::Chc). We could detect two different, apically enriched, signals: a diffuse one, resembling BicD distribution, and a more robust enrichment in one or sometimes two dots per cell that corresponded to the centrosomes as confirmed by their colocalization with the centrosomal marker Cnn (Fig. 1C, Supplementary Fig. S1B-C). Both immunostaining of Chc fusion proteins (Fig. 1C, Chc::V5) and live imaging of embryos expressing fluorescent Chc (Fig.1D and Supplementary Fig. S1D) revealed a dynamic localization of Chc during the cell cycle. Chc was distributed in a dotted pattern in the cytoplasm during the early syncytial divisions and enriched at the centrosomes and pericentrosomal regions during the entire cell cycle. During mitosis, Chc becomes associated also with the astral microtubules and the mitotic spindles (Fig. 1D, Supplementary Fig. S1D). Chc was also observed enriched during cellularization near the plasma membrane between the nuclei, probably marking the sites where endocytic vesicles start to form (Fig. 1C) (Sokac and Wieschaus, 2008). A similar localization pattern was observed for the *Drosophila* Clathrin light chain (Clc) during embryogenesis (Supplementary Fig. 1E).

We conclude that BicD and Chc associate with both the mitotic spindles and the centrosomes during mitosis. Thus, the Chc/Clc complex´s localization to the mitotic apparatus appears to be conserved between *Drosophila* and mammalian cells (Royle et al., 2005). Interestingly, mammalian BicD1 and BicD2 have been shown to be present at the centrosomes in mammalian cells as well (Fumoto et al., 2006). Therefore, our data suggest that *BicD* might play a yet unidentified, but evolutionary conserved role at the mitotic spindle.

deGradFP knockdown of BicD::GFP reveals a novel, essential role for BicD during early embryogenesis

Although *BicD*^{mom} flies lay embryos with mitotic defects, the numbers with which these progenies survive are too small for phenotypic analyses. Thus, we designed a strategy to knock down directly the BicD protein in early embryos using the deGradFP technique (degrade Green Fluorescent Protein), a method to target fusion proteins with GFP for destruction or inactivation (Caussinus et al., 2011). For this, we took advantage of the functional genomic *BicD::GFP* construct (Paré and Suter, 2000) and constructed a new version of the deGradFP that is specifically active during embryogenesis but not oogenesis. We cloned the NSlmb-vhhGFP4 sequence (that comprises the F-box domain contained in the N-terminal region of the *Drosophila* supernumerary limbs (Slmb) protein fused to the GFP-binding nanobody VhhGFP4 sequence) described by Caussinus *et al.* (2013) under the *hunchback* (*hb*) minimal maternal promoter containing the 5'-UTR leader of the maternal 3.2 Kb *hb* transcript and combined it with the *bcd* 3'-UTR (Fig. 2A) following the strategy used by Schulz and Tautz who used this to induce an artificial Hb gradient in embryos (Schulz and Tautz, 1995).

The *hunchback* promoter is transcribed during late oogenesis, and the mRNA will be loaded into eggs and embryos. The *bcd* 3' UTR promotes mRNA localization to the anterior pole of the oocyte and egg, and it will foster translation upon egg-laying only (Berleth et al., 1988; Driever and Nüsslein-Volhard, 1988; Sallés et al., 1994). The deGradFP construct should therefore be expressed in the early embryos but not during oogenesis. We will refer to it as *hb-deGradFP* (Fig. 2A). We corroborated the enrichment of the *deGradFP* mRNA in the embryo´s anterior region from egg laying untill before cellularization (Fig. 2B). This indicated that the cloned 3'-UTR of *bcd* was sufficient to direct anterior mRNA localization. However, immunostaining experiments to detect *deGradFP* expression using an anti-Lamma IgG antibody revealed that the Vhh-GFP was distributed in the entire embryo and did not form an A-P gradient (Fig. 2C). It thus appears that the deGradFP is stable and that it can diffuse or is streamed to the rest of the embryo. Even though our plan to use the embryo´s posterior half as an internal control did not materialize, *deGradFP* was expressed in very early embryos. We further used it to knock down the BicD::GFP protein in young embryos to study *BicD´*s role during the very early nuclear divisions and spindle assembly.

Two copies of a *BicD::GFP* construct rescued the sterility phenotype and the embryonic development arrest of *BicD* loss-of-function mutant females (*BicD::GFP, BicD*^{null} homozygous females) (Fig. 2D-E). However, when these females expressed 2 copies of the *hb-deGradFP* construct (*BicD::GFP, BicD*^{null} ; *hb-deGradFP* homozygous females), 75% of their progeny failed to developed to late embryonic stages and did not hatch into larvae,

showing arrest in the very early meiotic and/or mitotic divisions as observed in embryos laid by *BicD*^{mom} females (Fig. 2D-E, Supplementary Fig. S1A). In the following, we will refer to these mothers and their progeny as *BicD*$^{hb\text{-}deGradFP}$. Embryos laid by females that expressed two copies of the *hb-deGradFP,* but also a wild-type *BicD*$^{+}$ (*BicD::GFP, BicD*^{null} / + (CyO); *hb-deGradFP*), did not show development problems, indicating that high levels of *hb-deGradFP* expression are not deleterious for development on their own (Fig. 2D-E). *BicD*$^{hb\text{-}deGradFP}$ females displayed normal ovaries, and their BicD::GFP protein levels were not noticeably reduced in the ovary as assayed by immunofluorescence and Western blotting (Fig. 2F-H). These results confirmed that the *hb-deGradFP* construct is not active during oogenesis. In contrast, in young *BicD*$^{hb\text{-}deGradFP}$ embryos, the BicD::GFP signal was clearly reduced in the entire embryo (Fig. 2G), and BicD::GFP protein levels were downregulated by 50% (Fig. 2I). The fact that only a 50% reduction in the levels of BicD::GFP protein produces already visible phenotypes may be due to different reasons. One possibility is that the deGradFP might bind BicD::GFP, functionally inactivating the protein before sending it to degradation. On the other side, a BicD::GFP fraction may be already inactive and accumulates in the cell in a way that cannot get attacked by the deGradFP.

Measuring the expression of the *hb-deGradFP* construct by Western blotting revealed that it was indeed much higher expressed in early embryos, although low levels of expression were also seen in ovaries (Fig. 2H, I). This expression was also observed in ovaries dissected in Robbs medium, a hypotonic medium that is normally used to avoid oocyte activation (Supplementary Fig. 2A). Although we cannot rule out that some old egg chambers are activated during dissection due to physical activation, it is also possible that the sequences in the *bcd* 3'-UTR are not sufficient to fully control translation in the context of the maternal *hb* promoter and its 5'-UTR. Stage 14 (S14) oocytes are normally arrested in Metaphase I of meiosis I, till the oocyte becomes activated by its passage through the oviduct. Because *BicD*$^{hb\text{-}deGradFP}$ embryos arrest very early during development, we also wanted to test whether oogenesis expression of the *hb-deGradFP* construct might have affected meiosis by a potentially small reduction of *BicD* activity (Supplementary Fig. S2B-C). However, *BicD*$^{hb\text{-}deGradFP}$ S14 oocytes showed no evident problems in spindle formation or chromosome alignment in meiotic metaphase I (Supplementary Fig. S2B-C). These data suggest that the early embryonic arrest we observed in *BicD*$^{hb\text{-}deGradFP}$ individuals is not due to earlier meiotic defects during late oogenesis.

***BicD* is required for the cell cycle arrest of the male and the female meiotic products, and for pronuclear fusion**

Reduced BicD levels in young embryos led to an early arrest of development (Fig. 3), pointing to an essential function for *BicD* at this developmental stage. To learn more about this function, we collected 30-40 min old, fully viable control embryos and $BicD^{hb\text{-}deGradFP}$ embryos and analysed them for developmental defects (Fig. 3A). Twenty-five minutes after the eggs were laid, control embryos finished the 2nd mitotic division and contained at least four zygotic nuclei. At this early stage, normal zygotic nuclei (that are formed after the fusion subsequent division of the female and male pronuclei) reside in the interior of the embryo and, the three remaining female meiotic polar body products (mostly, but not always, fused into one rosette shaped nucleus) stay at the embryonic surface. Indeed, most embryos laid by control mothers (*BicD::GFP,* $BicD^{null}$ or *BicD::GFP,* $BicD^{null}$ / + (CyO); *hb-deGradFP)* developed normally, displaying more than four zygotic nuclei with normally looking mitotic spindles (Fig. 3A-B). However, embryos laid by $BicD^{hb\text{-}deGradFP}$ mothers arrested mostly in early development showing spindle defects (Fig. 3A, C). They mainly displayed centrally located dividing nuclei with spindle-like structures that appeared abnormal. Around 25% of these embryos were classified as "arrested with centrosomes" because they were positive for Cnn staining (Fig. 3A, an example in Fig 3Ca). These embryos contained at least one spindle displaying clear and sometimes fragmented staining for the centrosomal marker centrosomin (Cnn) at the spindle poles. Additionally, they frequently also displayed free centrosomes, positive for Cnn and associated with α-tubulin, but not with DNA (example in Fig. 3Ca1). Another 35% of the $BicD^{hb\text{-}deGradFP}$ embryos possessed one or more internal acentrosomal spindle and all these spindles were negative for Cnn staining and were classified as "arrested, acentrosomal" (Fig. 3A, Cb).

Since centrosomes are inherited from the father, embryos arrested in early development, but displaying at least one Cnn positive spindle or free Cnn positive signals, are expected to have developed from fertilized eggs that either underwent aberrant meiosis or were arrested in the very first mitotic divisions. By contrast, embryos that arrested development without displaying Cnn signal may represent unfertilized eggs that underwent aberrant meiosis. To unambiguously discriminate between fertilized and unfertilized embryos, we additionally either monitored the presence of the sperm tail or the X and Y chromosomes. Consistently, eggs containing at least one spindle with centrosomes and or acentrosomal like spindles plus free centrosomes were mostly marked by the presence of the sperm tail (Supplementary Fig. S3A-B). In contrast, embryos displaying "acentrosomal"-like spindles and no free centrosomes rarely displayed any of these sperm tail markers, indicating that they more likely represent unfertilized eggs with aberrant meiotic products (Supplementary Fig.

S3A-B). *BicD*$^{hb\text{-}deGradFP}$ mothers are weak and easily stick to the food. This defect likely affected their mating behavior and might be the reason for the presence of unfertilized eggs laid by these females.

The second approach to discriminate between fertilized and unfertilized eggs was based on detecting the presence of the X and Y chromosomes by DNA *in situ* hybridization. Male embryos (marked by the presence of the Y) developed only from fertilized eggs. Male embryos from control mothers showed one dot-like signal for the X chromosome and one signal for the Y in each zygotic nucleus, and these nuclei were located in the interior of the embryo. The three polar bodies, formed after the two meiotic divisions, normally fused into a single polar body that was marked by the presence of the 3 X chromosomes (Fig. 3D). In contrast, arrested male embryos laid by fertilized *BicD*$^{hb\text{-}deGradFP}$ females had one internal spindle marked only by the presence of the Y chromosome and no X chromosome signal, indicating that no pronuclear fusion had occurred and that a spindle still formed from the paternal pronucleus (Fig. 3E). The male pronucleus seemed to have undergone one additional round of replication since metaphase nuclei containing two dots of the Y chromosome signal can be observed in such embryos (Fig. 3E2). They also contained one or several acentrosomal nuclei marked frequently by the presence of several dots of X chromosomal staining, suggesting that the polar bodies did not arrest in metaphase II as they normally do but underwent several cycles of DNA replication instead (example in Fig. 3E1). These results show that *BicD* is required for the female and male pronucleus´ cell cycle arrest and for pronuclear fusion.

BicD is needed for replication arrest in polar bodies and for their rosette formation

To test for an essential function of *BicD* during the final phase of the meiotic divisions, we crossed *BicD*$^{hb\text{-}deGradFP}$ and control females to sterile XO males. This cross caused the females to lay unfertilized eggs. (Fig. 4). In wild-type unfertilized eggs, egg activation is triggered by passage through the oviduct, and this causes the eggs to complete meiosis II. In collections of 0-1h old unfertilized control eggs, we observed from 1 to 4 rosette-like nuclei. These are intermediate stages of the four meiotic products´ fusion process, which ultimately fused to form a single, rosette-shaped nucleus. Their presence indicates that the egg completed meiosis II. These rosette-shaped nuclei were also marked by the presence of a total number of 4 dots of X-chromosomal signal per egg, which arise from each of the four meiotic products (Fig. 4A, examples in Fig. 4B). In contrast, *BicD*$^{hb\text{-}deGradFP}$ unfertilized eggs contained one to several nuclei forming spindle like structures, mostly with the appearance of multipolar spindles. Additionally, their DNA did not create a rosette structure that would be typical for a metaphase arrested state. Instead, these nuclei displayed partially decondensed chromatin and

they were irregularly shaped and lacked the α-tubulin staining ring that surrounds the DNA rosette in control eggs (Fig. 4A,C). Furthermore, the X-chromosomal probe produced more than the normal four signal dots per egg, in both eggs containing only one nucleus (Fig. 4C-c) and in eggs containing several nuclei and spindles (Fig. 4C-c'). We observed eggs with more than four meiotic nuclei (like in Fig. 4Cc'), indicating that *BicD*$^{hb\text{-}deGradFP}$ eggs show over-replication of the meiotic products. The probe used for the DNA *in situ* experiments recognizes a repetitive region on the X-Chromosome present along 3 to 3.5 Mb. The fact that this probe detected more than four signals in each *BicD*$^{hb\text{-}deGradFP}$ egg, and that these signals showed different brightness and sizes might also suggest that the DNA has become fragmented and or more decondensed and that it did not arrest in a metaphase-like state as in the normal rosette structures. This replication, decondensation and or fragmentation of the meiotic DNA was not restricted to the sex chromosomes because we observed analogously additional signals when using a probe for the 2nd chromosome (Supplementary Fig. S4). All together, these results indicate that BicD is required for both the cell cycle arrest and the formation of the typical rosette-like structures of the polar bodies.

Role of BicD in SAC and metaphase arrest of female meiotic products

After meiosis II is completed, *Drosophila* polar bodies remain arrested in a metaphase-like state. Thus, we analyzed if the meiotic products in *BicD*$^{hb\text{-}deGradFP}$ unfertilized eggs were properly arrested in metaphase by monitoring the presence of the mitotic marker Phospho-Histone 3 (PH3). In wild-type unfertilized eggs, the four meiotic products, which fused into a single rosette, showed strong PH3 staining along the entire chromosomes, indicating that they were arrested in a metaphase-like state (Fig. 4Da-Ea). In contrast, in *BicD*$^{hb\text{-}deGradFP}$ eggs showing one rosette-like structure, the PH3 staining was not localized along the entire chromosomes but only enriched at the pericentromeric region (Fig. 4 Db-Eb) instead. Moreover, compared to control eggs, rosette-like structures in *BicD*$^{hb\text{-}deGradFP}$ eggs showed an increased number of CID-positive dots suggesting that female meiotic products underwent extra rounds of DNA replication (compare Fig. 4Da with 4Db).

Rosette-like structures in *BicD*$^{hb\text{-}deGradFP}$ eggs did also not form the typical tubulin ring surrounding the chromosomes observed in wild-type eggs, and interestingly, DNA extended beyond this tubulin ring, and this DNA was negative for PH3 staining (Fig. 4Ea, b, c). In the normal situation, Histone H3 phosphorylation starts in pericentromeric heterochromatin regions at the onset of mitosis and then spreads along the entire length of chromosomal arms, reaching its maximal abundance during metaphase. This is then followed by a rapid decrease upon transition to anaphase (Sawicka and Seiser, 2012). Thus, PH3 staining confined to the pericentromeric region in *BicD*$^{hb\text{-}deGradFP}$ polar bodies suggests that these nuclei are not

properly arrested or are released from metaphase arrest. Furthermore, *BicD*$^{hb\text{-}deGradFP}$ eggs possessing several meiotic products (Fig. 4Ec,c'), showed that not all of these nuclei were positive for PH3 staining (Fig. 4Ec2-3,c') further strengthening the idea that these nuclei are over-replicating due to a failure to arrest in metaphase.

The metaphase arrest of polar bodies has been shown to depend on the activation of the spindle assembly checkpoint (SAC) pathway (Défachelles et al., 2015; Fischer et al., 2004; Pérez-Mongiovi et al., 2005). We, therefore focused on analyzing the localization of two well-conserved orthologs of the SAC pathway, BubR1, and Mad2 (Fig. 5). These proteins associate with unattached kinetochores and in the case of BubR1, also to kinetochores lacking tension. By inhibiting the anaphase-promoting complex (APC/C) they are essential to maintain the metaphase arrest. BubR1 was clearly present at polar body kinetochores in the wild type (100%, n=23) and in the control BicD::GFP rescued eggs (93%, n=27) (Fig. 5Aa). However, in 43% of the *BicD*$^{hb\text{-}deGradFP}$ eggs, the meiotic products failed to recruit BubR1 to the kinetochores (n=35). The absence of BubR1 from the polar body kinetochores was observed in eggs where polar bodies were fused into a single rosette (Fig. 5Ab) and in eggs showing many additional meiotic products (Fig. 5Ad, d'). The rest of the *BicD*$^{hb\text{-}deGradFP}$ eggs showed either normal BubR1 recruitment (40%) or only a weak signal for kinetochore BubR1 (17%, Fig. 5Ac). These data indicate that the failure to activate or maintain the metaphase arrest of polar bodies in the absence of BicD is probably due to a failure to recruit the SAC components to the kinetochores or maintain their association. The fact that half of the polar bodies still recruited SAC components might also suggest that these nuclei are cycling in and out of the metaphase arrest, duplicating their chromosomes. Similar results were obtained for Mad2, where 69 % of the *BicD*$^{hb\text{-}deGradFP}$ eggs analyzed did not show recruitment of Mad2 to the polar bodies (n=48; Fig. 5B). Altogether, these results suggest that in *BicD*$^{hb\text{-}deGradFP}$ eggs, the meiotic II products do not correctly arrest in metaphase due to a failure to activate or maintain the SAC.

Chc is enriched at the meiotic spindle

Since embryos with reduced levels of BicD showed meiotic defects after release from MII arrest, we asked whether BicD and its interactor Chc, which we found previously to localize to mitotic spindles, are also present at the meiosis II spindle. Indeed, Chc::mCherry clearly localized to the meiotic spindle (Fig. 6A). BicD and the BicD::GFP, were also present around the meiotic spindle. However, compared to the signal intensities in the cytoplasm, no enrichment could be observed, even though a specific BicD signal was observed in the meiotic spindle region (Fig. 6B).

D-TACC, Msps and Clc localization to the tandem meiotic spindles depends on BicD

The analysis of Chc distribution turned out difficult due to the lack of useful antibodies for immunostaining. Localization of tagged proteins was also irreproducible due to the high cytoplasmic staining and side effects of tagged Chc proteins overexpression (Fig. 9F-G). However, mammalian Chc forms a complex with the two proteins TACC3 (transforming acidic coiled-coil containing protein 3) and ch-TOG (colonic and hepatic tumor overexpressed gene) at the mitotic spindles. The presence of these proteins at the spindle is interdependent and is needed for stabilizing the kinetochore fibres by forming inter MT-bridges that are essential for normal progression through mitosis in vertebrate cell (Royle, 2012; Royle et al., 2005). We then decided to follow the localization of the *Drosophila* homologs of TACC3 (called D-TACC) and ch-TOG (called Msps (Mini spindles)) at the meiotic spindles. To pinpoint the first meiotic defects, we focused on the very early stages of meiosis II in eggs that were just released from the MI arrest. In wild-type MII and anaphase II (AII) spindles, D-TACC and Msps were present on tandem spindles, and they were enriched at the central aster (Fig. 6C, D arrowheads). In both metaphase and anaphase, D-TACC is additionally weakly enriched at the spindles´ equator, where the MT plus ends are located (Fig. 6C, arrows). On the other hand, Msps was clearly enriched along both arms of the tandem spindles but stained more strongly the minus ends at the spindle poles (Fig. 6D, arrows). In $BicD^{hb\text{-}deGradFP}$ embryos, D-TACC and Msps localization along the tandem spindles was generally clearly reduced compared to the control spindles (Fig. 6C, D). However, like in control spindles, D-TACC and Msps still showed enrichment at the central aster in $BicD^{hb\text{-}deGradFP}$ embryos (Fig. 6C, D).

To follow clathrin localization more directly, we stained the embryos for Clathrin light chain (Clc). In metaphase II, Clc localized to the spindle and the central aster (Fig. 6E). However, Clc showed a robust signal in the cytoplasm, too, which made spindle signal detection more challenging. Due to the meiotic spindle´s variable position, and the depth of the sample, it was not possible to analyze Clc localization at the different regions of the meiotic spindles just by analyzing the Z-stack maximal confocal projection images. The high cytoplasmic signal in the first planes masked the localization at the spindle in the deeper planes. However, applying a bleach correction to the Clc signal in each Z-frame (see Methods), allowed us to detect the miss-localization of Clc on the tandem spindles of $BicD^{hb\text{-}deGradFP}$ eggs. Similar to the localization of D-TACC and Msps, Clc showed an unusual, strong accumulation at the central aster compared to the levels observed along the spindle (Fig. 6E, E'). These results suggest that BicD is needed to properly localize D-TACC and Msps on the meiotic II spindles, most probably through its effect on localizing or transporting Clathrin along microtubules.

Evidence for mutually exclusive complexes of BicD/Chc and D-TACC/Chc

BicD and Chc proteins form a complex and have been shown to interact directly in *Drosophila* (Li et al., 2010; Vazquez-Pianzola et al., 2014). In mammals, Chc interacts directly with TACC3, and the interaction depends on the phosphorylation of Ser^{552} of TACC3 by Aurora A (Fu et al., 2010; Lin et al., 2010). However, it is not known whether the interaction between D-TACC and Chc is conserved in *Drosophila*. We, therefore, tested the interaction in a yeast 2-Hybrid (Y2H) assay and by immunoprecipitation experiments (Fig. 7A-B). Indeed, full-length *Drosophila* Chc interacts with D-TACC in both assays.

In the mammalian system, the minimal region of Chc22 that interacts with mammalian TACC3 was identified as amino acids 331-542 (Lin et al., 2010). However, the corresponding region of *Drosophila* Chc (aa 329-542) did not show an interaction with D-TACC in our assays (Fig. 7A). The same Chc fragment was also unable to bind BicD (Supplementary Fig. S5A). However, a longer fragment of *Drosophila* Chc that contains additional residues at the C-term (aa 329-803) interacted with D-TACC almost as strongly as the full-length protein (Fig. 7A). Interestingly, this fragment was shown previously to contain the minimal region needed to bind *Drosophila* BicD (Li et al., 2010) (Supplementary Figure S5B). The same region of Chc interacted in our assays with the BicD CTD (C-terminal domain), a truncated version of BicD that normally interacts stronger with its cargoes because it does not contain the BicD fold back domain (Supplementary Fig. S5B) (Li et al., 2010). Since the sequences required for the binding of *Drosophila* Chc to D-TACC and to BicD are overlapping, Chc/BicD and Chc/D-TACC might only exist as mutually exclusive protein complexes. However, because Chc normally acts as a trimer, higher-order complexes of the three Chc molecules could theoretically contain BicD or D-TACC, or both. Surprisingly, the interaction of Chc with D-TACC was not abolished when the conserved Ser residue targeted by the Aurora A kinase was mutated to Alanine (Ser^{863} in D-TACC, corresponds to Ser^{552} of the human protein, Fig. 7A, Supplementary Fig. S5C). Nevertheless, the phosphomimetic mutation Ser^{863} > Asp^{863} D-TACC increased its interaction with full-length Chc (Supplementary Fig. S5C). These results suggest that phosphorylation of Ser^{863} may not be a prerequisite for the interaction of full-length D-TACC with Chc at least in the Y2H system. Still, it could enhance the interaction during mitosis and meiosis when the kinase is active, suggesting a significant and conserved role for the D-TACC/Chc complex and D-TACC phosphorylation during evolution.

The interaction of D-TACC with full-length Chc was even observed under very stringent Y2H conditions (medium -L, -W, -H, -a; Supplementary Figure S5C). In contrast, the interaction between Chc and BicD was only visible under less stringent conditions (medium -L, -W, -H +3 mM 3AT; Supplementary Fig. S5A, (Cagney et al., 2000)),

suggesting that Chc interacts stronger with D-TACC than with BicD in this system. This is also supported by the immunoprecipitation experiments using embryo extracts. Using extracts expressing a Myc::Chc fusion protein, Myc::Chc was observed at low levels in BicD IPs. In contrast, the presence of BicD was not detected in the reverse IPs (with anti-Myc antibodies) as previously reported (Fig. 7B) (Vazquez-Pianzola et al., 2014). This is conceivable due to their weak interaction or because the Myc tag interferes with the binding sites. In contrast, D-TACC was strongly pulled down with anti-Myc antibodies from extracts containing the Myc::Chc fusion protein. On the other hand, no interaction was observed between D-TACC and BicD either by IP or using the Y2H system (Fig. 7B and Supplementary Fig. S5D).

D-TACC is required, like BicD, for pronuclear fusion and cell cycle arrest of the male pronucleus

Mothers expressing the mutant *d-tacc* allele *d-tacc*^{1} are sterile. They lay eggs with reduced D-TACC protein levels, and the embryos arrest development early on (Gergely et al., 2000). The analysis of the 70% of the embryos that completely failed to develop suggested that they were arrested in the first mitotic divisions. We performed DNA *in situ* hybridization experiments to test for the X and Y-chromosomes´ presence in these mutant embryos. Whereas wild-type male embryos showed signals for both chromosomes in each of their zygotic nuclei (Fig. 8A), most of the male embryos laid by *d-tacc*^{1}*/ Df(3R)110* females had one internal nucleus strongly marked with two dots corresponding to the Y-chromosome and no X-chromosomal signal (Fig. 8B, upper panel, arrow) suggesting that the male pronucleus has undergone an additional S-phase. X-chromosome signals strongly marked the remaining embryonic nuclei. Even though they showed an additional, unspecific weak signal for the Y-chromosome that is also observed in the wild-type embryos (see figure legend), this pattern seems to represent polar bodies fused into two nuclei with a normal amount of four dots of X. A smaller fraction of male embryos displayed many Hoechst-positive nuclei-like structures marked only by the presence of the Y-chromosome (Fig. 8B, lower panel). No X-chromosome signal was evident in them. These embryos also contained polar bodies fused into one to four rosette-like nuclei marked by the presence of X-chromosome signals. These data show that in embryos with reduced TACC activity levels (Fig. 8), pronuclear fusion is compromised, and the paternal DNA undergoes additional rounds of replication as we observed in *BicD*$^{hb\text{-}deGradFP}$ embryos (Fig. 3D-E). However, unlike what we observed in *BicD*$^{hb\text{-}deGradFP}$ eggs (Fig. 3D-E), in *d-tacc*^{1}*/ Df(3R)110* embryos, we did not detect additional female meiotic products and the female-derived nuclei always displayed 4 X-chromosomal signals in total, indicating that the female meiotic products did not undergo an extra round of replication (Fig. 8B). Altogether,

these data show that in very early development, BicD and D-TACC are involved in common pathways that regulate pronuclear fusion and metaphase arrest of the male pronucleus.

***BicD* is needed for correct bipolar spindly assembly and centrosome integrity in *Drosophila* tissue culture cells**

Because embryos with reduced levels of BicD were arrested before zygotic divisions, we were unable to analyze BicD and Chc roles during embryonic mitosis. Thus, we decided to study the role of BicD in mitosis in *Drosophila* tissue culture cells. Efficient depletion of BicD, Chc and Clc in S2 cells was observed four days after RNAi treatment (Fig. 9A). Depleting either BicD, Chc, or Clc caused an increase of cells containing more than two centrosomes or fragmented centrosomes compared to cells treated with a control RNAi against GFP (Fig. 9B). An increase of cells showing multipolar spindles was also observed upon RNAi treatment against these mRNAs (Fig. 9B). Examples of the phenotypes observed are depicted in Fig. 9C. The observed increase in mitotic phenotypes was similar to the rates observed in human cells (Foraker et al., 2012). The fact that knockdown of *BicD, Chc,* and *Clc* showed similar mitotic defects suggests that these interacting proteins are needed for the same steps during mitosis.

Double KD of *Chc* and *Clc* neither enhanced nor rescued the defects observed upon single KDs (Fig. 9D-E, compare with Fig. 9B). This result is consistent with the fact that single KDs of either Clc or Chc, reduced the levels of both proteins as observed by WB (Fig. 9A and Supplementary Fig. S6). On the other hand, double knockdown of either *BicD* and *Chc* or *BicD* and *Clc* did not enhance the mitotic defects observed upon single knockdowns but partially rescued them (compare Fig. 9D-E with Fig. 9B). These results are consistent with the hypothesis that reducing the levels of *Chc* or *Clc* may partially rescue the phenotypes observed upon *BicD* KD since less Clathrin will become mislocalized on the spindle.

***In vivo* importance of proper BicD/Clathrin ratio**

The *in vitro* experiments suggested that the cellular balance between BicD and Clathrin might be necessary during mitosis. We tested this *in vivo* by overexpressing *Chc* in embryos with slightly reduced functional BicD and found that this indeed enhanced the phenotype (Fig. 9F-G). Homozygous null females were rescued with two copies of the BicD::GFP transgene and expressing only one copy of the *hb-deGradFP* construct *(BicD::GFP, BicD*^{null} ; *hb-deGradFP-bcd 3'UTR/+)* laid embryos that developed normally and hatched into larvae (Fig. 9F-G). However, when these females also expressed a copy of a *Chc* transgene under the control of the strong maternal tubulin promoter, 80% of their progeny failed to hatch as larvae and, instead, arrested in early development (Fig. 9F-G). Overexpression of this Chc construct

alone did not produce visible phenotypes in embryos, suggesting that high levels of Chc in a background that does not allow correct localization of Chc along MTs, is responsible for the phenotype.

Requirements for meiosis and pronuclear fusion for *C. elegans bicd-1*, *chc-1 and tac-1*

Our results indicate that pronuclear fusion requires *BicD* and *tacc* in *Drosophila*. These proteins might have a direct role in pronuclear fusion or, alternatively, be required for previous steps of oocyte formation, as BicD is necessary for normal completion of meiosis II. To find out whether BicD and the components of the Clathrin/TACC/ch-TOG complex play a conserved role in meiosis and pronuclear fusion, we turned to *C. elegans*, which, besides, allowed us to study these processes in real-time (Laband et al., 2018).

In a normally developing zygote, the female pronucleus lies in the anterior part of the embryo while the male pronucleus and its two associated centrioles define the posterior pole (Fig. 10A). Because the female pronucleus moves faster towards the posterior pole than the male pronucleus moves in the opposite direction, the two nuclei meet in the embryo´s posterior half. After centration and rotation, both nuclei move anteriorly, and the first mitotic spindle forms around the center of the zygote along the A-P axis. This process is readily visible in strains expressing histone H2B::mCherry and α-tubulin::GFP. Almost all embryos that were grown on either regular food (6/6) or control RNAi food supplied with empty vector (14/15) showed the expected progression from meiosis to the formation of the first mitotic spindle. (Fig. 10A).

Next, we followed pronuclear fusion in knock-out mutants and or RNAi knock-downs of the homologs of *tacc, Chc* and *BicD* (*tac-1, chc-1, and bicd-1*, respectively) (Kamath and Ahringer, 2003; Laband et al., 2018). Knock-down of *tac-1* led to both meiosis and pronuclear fusion defects (Fig. 10B-C), as previously described using DIC microscopy (Bellanger et al., 2007). Two out of five *tac-1*(*RNAi*) embryos showed abnormal meiosis with delayed polar body extrusion and no pronuclear fusion. The male pronucleus formed a spindle on its own at the posterior pole, and both pronuclei met at the posterior pole forming a common spindle without pronuclear fusion (Fig. 10B). In the other embryos, meiosis appeared normal, yet female pronuclear migration was defective, and pronuclei similarly did not fuse (2/5 embryos analyzed). In these embryos, the male pronucleus formed a spindle at the posterior pole, while the female pronucleus never migrated to the posterior (Fig. 10C). Together, this suggests a conserved role for the *tacc* homolog *tac-1* in pronuclear fusion (Fig 10B-C).

Most homozygote *chc-1(tm2866)* null mutant progeny did not hatch (6/10). The animals that hatched arrested development at various stages. It is possible that these managed

to survive to hatch with a maternal contribution from their balanced mother. Laid embryos displayed an abnormally elongated shape. Similarly, animals fed with *chc-1* dsRNA food looked sick and carried few progenies in the uterus. In the few living *chc-1* (RNAi) embryos, we observed arrested meiotic metaphases with a single meiotic spindle (2/6 embryos; Fig. 10F) and lack of pronuclear fusion with delayed migration and lack of centration of the female pronucleus (2/6 embryos; Fig. 10D). Additionally, one embryo showed a recapture of the polar body by the mitotic spindle followed by its nuclear fusion to the anterior blastomere of the 2-cell stage (Fig. 10G). The remaining embryo showed normal development. Together, this highlights the importance of *C. elegans chc-1* for oogenesis and development, as observed in *Drosophila Chc* (Vazquez-Pianzola et al., 2014).

Finally, we tested the phenotype of the *C. elegans BicD* homolog. 8 out of 10 *bicd-1(tm3421)* homozygous embryos did not hatch. This is consistent with *bicd-1* being an essential gene like *chc-1*. Moreover, 20% of hatched animals died at the adult stage without progeny, suggesting again that the maternal contribution rescued their embryonic development. Feeding animals with dsRNA directed against *bicd-1* led to delayed pronuclear migration of the female pronucleus in a fraction of the embryos (3/10; Fig. 10E) and, although both pronuclei ultimately met at the posterior, they neither fused nor moved towards the center of the embryo, a phenotype similar to the one observed in *chc-1(RNAi)* animals (compare Fig. 10D and E). The fact that meiosis and or pronuclear migration and fusion are compromised when *tac-1*, *chc-1 and bicd-1* function is compromised in *C. elegans* and *Drosophila* embryos, suggest an evolutionarily conserved role for the three proteins for meiosis and pronuclear fusion.

DISCUSSION

A conserved role of Chc in spindle assembly in lower eukaryotes

Vertebrate Chc has an essential function during mitosis as part of the Chc/Tacc/ch-Tog complex. However, while Chc is conserved across eukaryotes, reports of its role at the mitotic spindle have been limited to vertebrates (human, rat, mouse, and *Xenopus*) and plants (Fu et al., 2010; Lin et al., 2010; Royle et al., 2005; Tahara et al., 2007; Yamauchi et al., 2008). Here, we found that *Drosophila* Chc is present at mitotic and meiotic spindles, and that depletion of Chc in *Drosophila* cells leads to aberrant mitosis. We also found that *Drosophila* Chc interacts directly with D-TACC and that knocking down *tac-1* and *Chc-1* homologs in *C. elegans* leads to meiotic and early mitotic phenotypes. Our observations show that these proteins have a conserved function at invertebrate spindles and that they probably act as part of a conserved complex.

A useful strategy to study the effect of lethal or female sterile mutations in early embryogenesis reveals novel requirements for *BicD* in meiosis

We also found that BicD, another partner of Chc, is also present at the mitotic spindles and that cells depleted of BicD also showed mitotic phenotypes. Since *BicD* ^{null} mutants rarely survive and are sterile, we set up a strategy based on the deGDradFP technique to assess its role during early embryonic divisions. The deGRadFP construct was expressed under the control of a maternal *hunchback* promoter and with *bcd* 3'-UTR sequences that prevent translation of the GFP nanobody mRNA until egg activation. Using this strategy, we discovered that *BicD* plays an essential role during early embryogenesis, where it is essential for meiosis II progression. Combined with the CRIPSP-Cas9 strategy first to produce functional GPF tagged versions of the proteins of interest, the construct designed in this paper could be useful to study the role of other female-sterile and lethal mutations during very early development (Nag et al., 2018).

BicD is involved in correct meiosis II spindle assembly and pronuclear fusion

Embryos with reduced levels of BicD arrest development displaying aberrant meiotic products and no pronuclear fusion. Furthermore, localization of the Chc partners, D-TACC, Msps, and Clc to the meiotic II spindle was compromised in embryos with reduced BicD levels. Thus, we discover a novel role for Chc and probably the Chc/D-TACC/Msps complex in forming the female *Drosophila* meiotic spindle. Knocking down in *C. elegans* embryos *tac-1* and *Chc-1* also led to meiosis problems, indicating a conserved role for this complex for the correct assembly of the female meiotic spindle. Our results also revealed an essential and conserved role for *Drosophila D-TACC* and *BicD* and *C. elegans chc-1, tac-1* and *bicd-1* for pronuclear fusion. This function might either be required indirectly, through its role in meiosis, and or the complex might play a more direct role in pronuclear migration, which is known to depend on Dynein and MTs in bovine, primate, and *C. elegans* embryos (Gönczy et al., 1999; Payne et al., 2003).

Connecting BicD to the SAC pathway

In higher animal cells, all kinetochores start mitosis unattached, and the checkpoint signal is constitutively present due to the recruitment of the SAC pathway components to kinetochores that are unattached or are under insufficient tension. The SAC complex is present until the checkpoint is satisfied, at which time it is shut off, and cells enter anaphase. One mechanism that triggers the checkpoint´s silencing is the movement of several checkpoint proteins from kinetochores along microtubules to the spindle poles in a dynein-dependent manner. In human

cells, depletion or chemical inhibition of Chc and the use of Aurora A inhibitors prevent the TACC/Clathrin complex from binding to the mitotic spindles. This affects K-fiber formation and leads to defective chromosome congression to the metaphase plate. As a consequence, the SAC becomes persistently activated (Rieder and Maiato, 2004; Royle et al., 2005). Impairment of MT motors, such as dynein, as well as interference with MT dynamics, persistently activates the SAC, too (Rieder and Maiato, 2004). The proteins involved in this process are highly conserved from yeast to humans, and although less robust, the SAC control has also been found to be active during meiosis (Marston and Wassmann, 2017).

Interestingly, in *Drosophila* mutants for several conserved orthologs of the SAC pathway (*Rod, mps1* and *BubR1*), polar bodies cannot remain in their SAC-dependent metaphase-like state and decondense their chromatin (Défachelles et al., 2015; Fischer et al., 2004; Pérez-Mongiovi et al., 2005). Furthermore, polar bodies have been shown to cycle in and out of M-phase, replicating their chromosomes. Two mechanisms could explain the replication and or decondensation of polar bodies observed in $BicD^{hb\text{-}deGradFP}$ embryos. Although we do not have any experimental evidence, BicD could be needed to recruit the SAC components to kinetochores directly. Alternatively, dynein motors have been shown to physically transport SAC components away from kinetochores along microtubules (Basto et al., 2004; Howell et al., 2001; Wojcik et al., 2001). Because normal BicD binds dynein, we expect that, if BicD acts as a link to transport SAC components, in the absence of BicD function, their movement way from the kinetochores would be affected, causing the SAC to remain persistently activated. However, based on our finding that BicD is needed to localize the TACC/Msps complex to the meiotic II spindles, we favor the hypothesis that in the absence of BicD, the stability of the K-fibers is compromised, and this leads to persistent activation of the SAC pathway.

Persistent activation of the SAC might lead to metaphase arrest, preventing anaphase onset and delay meiosis (D-Meiosis). However, at least during mitosis, this delay is known to be rarely permanent. Most cells that cannot satisfy the SAC, ultimately escape D-mitosis and enter G1 as tetraploid cells by a mechanism that is poorly understood (Rieder and Maiato, 2004). Similarly, mechanisms defining these cells´ subsequent fate that will either die or continue replicating are not well known (Rieder and Maiato, 2004). Thus, we suggest that in embryos with reduced *BicD* function, meiotic II kinetochore microtubule attachment might be compromised, and the SAC pathway constantly activated, thus delaying meiosis. However, at one point, they might escape the metaphase II arrest and enter into cycling in and out of M-phase, replicating their chromosomes and de-condensing their chromatin. The fact that meiotic products in $BicD^{hb\text{-}deGradFP}$ embryos show either no or only pericentromeric PH3 staining and that polar body nuclei are replicating, support the notion that these nuclei are on an in-out metaphase arrest phase. This is also supported by the finding that in around half of

668 the *BicD*$^{hb\text{-}deGradFP}$ embryos the meiotic products failed to stain for the SAC components
669 BubR1 and Mad2. That delaying of mitosis due to a persistently activated SAC might occur
670 also in mitotic embryos with reduced BicD levels is supported by the observation that in the
671 few *BicD*$^{hb\text{-}deGradF}$ embryos that go through the first mitotic divisions, most (70%) were found
672 to be in metaphase compared to the 20-30% control embryos that were in metaphase
673 (Supplementary Fig. S7).
674 BicD also interacts with Polo (Mirouse et al., 2006), a kinase that supports SAC
675 activation during mitosis by phosphorylating the key components of the pathway, Mps1
676 and PLK1, in different species (Conde et al., 2013; Espeut et al., 2015; Ikeda and Tanaka,
677 2017; Schubert et al., 2015). Interestingly, *Drosophila* embryos derived from *polo*^{1} mutant
678 mothers show abnormal meiosis II spindle assembly with compromised pronuclear fusion,
679 similar to what we observed in *BicD*$^{hb\text{-}deGradF}$ embryos (Riparbelli et al., 2000). However,
680 although *polo*^{1} polar bodies arrested in metaphase, like those in *BicD*$^{hb\text{-}deGradF}$ eggs, they
681 underwent many more rounds of division cycles populating the embryo surface in *polo*^{1}
682 mutants. We did not observe a BicD enrichment at kinetochores, suggesting that it might not
683 play a direct role in Polo recruitment and SAC activation at the kinetochores. However,
684 another intriguing hypothesis is that BicD may play a role in removing Polo from the
685 kinetochores to allow anaphase onset. Whether the disruption of the Polo-BicD interaction
686 contributes to some of the phenotypes we observed upon the BicD KD requires further
687 investigation and goes beyond the scope of this study.
688 Mitotic proteins that activate or inhibit the SAC, such as aurora A kinase and kinesin
689 spindle protein (KSP; also known as EG5), respectively, have been targets for developing
690 chemotherapy drugs (Jackson et al., 2007). Following activation or inhibition of the SAC
691 pathway, these drugs reduce tumor volume *in vitro* either by triggering cell death or inhibiting
692 tumor growth (Jackson et al., 2007; Rieder and Maiato, 2004). Recently, the small molecule
693 pitstop 2 that binds to the Chc terminal domain (TD) has been shown to induce mitotic
694 phenotypes consistent with clathrin inhibition. In addition, it displayed a specific anti-
695 proliferative and cytotoxic activity in dividing cancer cells, but not towards dividing non-
696 cancer cells (Kleist et al., 2011; Smith et al., 2013). However, pitstop 2 also inhibited clathrin-
697 mediated endocytosis, suggesting that it could have secondary effects in clinical trials, and it
698 was not as potent as the inhibitor of Aurora A, MLN8237, at inducing aberrant mitotic
699 phenotypes, inhibiting cell proliferation, and inducing cell death (Kleist et al., 2011). Pitstop 2
700 is not expected to affect the binding of Chc to TACC, because this interaction is mediated by
701 the Ankle domain of Chc. Thus, it will be interesting to know whether the generation of novel
702 analogs that target the Ankle domain of Chc, which binds to both BicD and TACC, will act as
703 a more potent anticancer drug.
704

Model for a role of BicD at the meiotic spindle

TACC and Msps orthologs are MT plus end-tracking proteins (Gutiérrez-Caballero et al., 2015; Lucaj et al., 2015; Nwagbara et al., 2014; Rutherford et al., 2016). In addition to phosphorylation of Ser^{552} of TACC3 by Aurora B, *Drosophila* D-TAAC is phosphorylated by Aurora A at Ser863. This phosphorylation allows D-TACC to interact directly with the minus ends of the MTs and to further recruit Msps to stabilize the MT minus ends (Barros et al., 2005; Lee et al., 2001). D-TACC interaction with the MT minus ends does not depend on Chc (Gutiérrez-Caballero et al., 2015). The direct association of the TACC/Msps complex with the minus end of MTs could explain why localization of clathrin, TACC, Msps is less affected in the central aster of the meiotic II spindles where both MT plus and minus end-proteins are enriched (Riparbelli and Callaini, 2005). Based in this and our findings, we also hypothesize that during assembly of the meiosis II spindle, D-TACC binds directly to the MT plus ends and becomes stabilized along the spindle by its interaction with Chc.

BicD, on the other hand, can also recruit Chc to the microtubules through its association with dynein, moving Chc towards the microtubule minus ends. In the absence of BicD, Chc cannot be recruited or moved in a minus end direction along the spindle. Thus, a D-TACC/Clathtin/Msps complex cannot be stabilized along the spindle or be dynamically active at the spindle, and its localization along the spindle becomes compromised. Although we did not find evidence for the ternary complex TACC/Chc/BicD, it is still possible that the three proteins are part of a larger complex because Chc normally acts as a trimer with Clc (triskelion). In this complex, each Chc might interact with either BicD or D-TACC. A mixed complex could be formed, and BicD might be essential for the movement of Chc and TACC/Chc along the spindle via the interaction of BicD/Chc in the same trimer. Since the interaction between D-TACC and Chc is stronger than the interaction between BicD and Chc, as our two-hybrid system data suggest, then, once near the spindle, formation of the complex between D-TACC and Chc at the spindle could be favoured, and the complex could stabilize the K-fibres. This could explain the fact embryos laid by mothers overexpressing Chc in a background were BicD is reduced down to levels that do not produce visible phenotypes on their own (one copy of the deGRadFP construct with two copies of BicD::GFP) are also arrested in early development. Limited BicD activity in these embryos might be insufficient to transport the high levels of Chc or the Chc/TACC complex efficiently to the minus ends of the MTs and to stabilize the complex along the meiotic spindle. This model can also explain the effects we observed in *Drosophila* cells. In this case, double knockdown of *Chc* and *BicD* produced fewer mitotic defects than the single knockdown of the same proteins. Reducing both proteins´ levels simultaneously could favor the movement of the complex since less Chc will be available for binding TACC and become un-localized.

To conclude, we found that the lack of BicD affects recruitment of the Clathrin/ D-TACC/ Msps complex to the spindle. This phenomenon might result in a loss of K-fibre tension that impairs normal SAC inactivation. Consequently, the meiotic products then would enter a continuous abnormal cycle of SAC activation and metaphase arrest, followed by a SAC deactivation and cell cycle progression, replicating their chromosomes. This model would explain the concomitant meiotic arrest phenotype, associated with abnormal replication of the meiotic products and early developmental arrest that we observed in *BicD*$^{hb\text{-}deGradFP}$ embryos. Thus, our results show that *BicD* performs a key activity in assembling of the meiotic spindle control apparatus.

MATERIALS AND METHODS

Drosophila stocks

P{matα4-GAL-VP16}, *Nos-Gal4:Vp16* ; *UAS-Clc::GFP*, *Histone::RFP* ; C(1;Y)^{1}, y^{1}w: y^{+}/0 and *C(1)RM, y^{1} v^{1}/0* stocks were obtained from the Bloomington *Drosophila* Stock Center. Flies containing the genome rescue transgenes p*CHC3+* (Bazinet et al., 1993) and *4C-CHC* (Kasprowicz et al., 2008), were kindly provided by C. Bazinet and P. Verstreken, respectively. *d-tacc*^{1} and *Df 3R(110),* covering the *tacc* locus, were provided by J. Raff (Gergely et al., 2000). *UAS-Chc::eGFP* and *UAS-Chc::mcherry* flies (Li et al., 2010) were provided by S. Bullock. Transgenic flies *pUASP-Chc-V5-K10-AttB*, and *pUASP-myc-chc-K10-AttB* were described previously (Vazquez-Pianzola et al., 2014). *Df(2L)Exel7068* (Exelixis) was used as *BicD* deficiency (BicD^{Df}). The *BicD*^{null} allele, *BicD*^{r5}, *Bic-D*^{mom}, and *BicD::GFP* were described (Paré and Suter, 2000; Ran et al., 1994; Swan and Suter, 1996; Vazquez-Pianzola et al., 2014). *White (w)* flies were used as controls.

For the production of unfertilized egg, virgin *w* females were crossed to *C(1;Y)*^{1}*, y*^{1}*w: y*$^{+}$*/0* males to generate XO males that are phenotypically normal but sterile. XO males were then crossed to virgin females of the desired phenotype. Eggs laid by these females were not fertilized.

DNA constructs and generation of transgenic flies

Generation of the flies expressing the *hb-deGRadFP* construct was as follows. The *Nslmb-vhhGFP4* sequence was PCR-amplified with specific primers bearing *BamHI* and *KpnI* sites using the plasmid pUAS-Nslmb-vhhGFP4 as template (Caussinus et al., 2011). Primer sequences were the following ones. Nano GFP sense-BamHI (GGATCCATGATGAAAATGGAGACTGACAAAAT)
and Nano GFP anti-Kpn (GGTACCTTAGCTGGAGACGGTGACCTGGGTG). PCR

products were subcloned into the same sites of the pCaSper-AttB vector to create the plasmid pCasper-AttB-Nslmb-vhhGFP4 (or pw+GFP nanobody). A 1.5 Kbp fragment of the *bicoid* 3'-UTR genomic region (Berleth et al., 1988) was amplified from a genomic library using specific primers containing KpnI and NotI restrictions sites. Primers were: bcd 3'UTR sense-Kpn I (GGTACCACGCGTAGAAAGTTAGGTCTAGTCC) and bcd 3'UTR anti-Not I (GCGGCCGCGCTAGTGCTGCCTGTACAGTGTCT). The insert was cloned by T-end ligation into the pCR2.1 TOPO vector and later subcloned into the KpnI/ NotI sites of pCasper-AttB-Nslmb-vhhGFP4 to generate the pCasper-AttB-Nslmb-vhhGFP4-bcd 3'-UTR construct (or pw+ GFP nanobody-bcd 3'-UTR). The minimal maternal *hunchback (hb)* promoter region together with the 5'-UTR leader of the maternal 3.2 Kb *hb* transcript were amplified using as template the Lac8.0 construct already described (Margolis et al., 1994) and kindly provided by Jim Posakony. Primers for this amplification contained flanking BglII and BamHI sites and were the following ones. Hb-pr-sense–BglII (AGATCTTCCGGATCAGCGGCGCTGATCCTGC), and Hb-pr-Anti-BamHI (GGATCCCTTGGCGGCTCTAGACGGCTTGCGGACAGTCCAAGTGCAATTC). Inserts were further cloned into the *BamHI* of Nslmb-vhhGFP4-bcd 3'-UTR to generate Hb-Nslmb-vhhGFP4-bcd 3'UTR (or pw+ Hb-GFP nanobody-bcd3'UTR). This final plasmid was injected into embryos containing the ZH-attP-14/3R-86F landing platform to generate flies expressing the *hb-deGradFP* construct.

The *Don Juan (Dj)::mCherry* construct to produce transgenic flies was generated as follows. mCherry region was PCR-amplified with primers containing BamHI and HindII sites using pC4-SqhP-mCherry plasmid as template (a gift from Romain Levayer). The reverse primer added a GS-rich region to use as a linker and the stop codon was removed. The amplified fragment was further subcloned into the BamHI/HindIII sites of the plasmid *pw+SNattB* (Koch et al., 2009) to generate the plasmid *pw+attB*-mCherry. The genomic region containing the minimal promoter, the 5'-UTR and the ORF of *Dj* gene was-PCR amplified from genomic fly DNA using primers containing EcoRI and BamHI sites, and cloned into the same sites of *pw+attB*-mCherry to generate the final construct *pw+attB - Don Juan (Dj)::mCherry*. This construct was further injected into flies containing the ZH-attP-52 / 3L-64A landing platform for transgenesis.

Hatching rate determination and embryo development

Hatching rates were scored as follows. Virgin females of the desired genotype were crossed to control *white* males. Females were allowed to lay eggs on agar plates for several hours or overnight. Around 100-200 embryos were marked in the plate and further developed for 48 h at 25^{o}C. After 48 h, embryos that did not hatch were counted. For scoring embryo

development, 2- to 5-h-old embryos were collected. Embryos were then fixed and stained to detect both α-tubulin and DNA to score the development stage.

Western blots

Preparation of ovaries for Western blots was as follows. Seven pairs of ovaries were collected in 20 µl of SDS-sample buffer, boiled for 2 min., vortexed for 15 sec., boiled for another 8 min. Finally, they were loaded onto an SDS –PAGE. Western blots were performed using mouse monoclonal anti-BicD antibodies (a mixture of 1B11 and 4C2, 1:10 dilution, (Suter and Steward, 1991), mouse anti-α-tubulin (1:2,000 dilution of the cell culture´s supernatant, Developmental Studies Hybridoma Bank (DSHB)), rabbit anti-mammalian Chc (1:500 dilution, (Hirst et al., 2009)), rabbit anti-GFP (1:3,000 dilution, Immunokontact), rabbit anti-Clc (1:3,000, (Heerssen et al., 2008)), mouse monoclonal anti-Myc 9E10 (1:5 cell culture supernatant, DSHB), and rabbit anti D-TACC (1:10,000 dilution, (Kao and Megraw, 2009)). Primary antibodies were detected using horseradish peroxidase-conjugated secondary antibodies (GE Healthcare). To detect the hb-deGRadFP construct expression, anti-llama IgG-heavy and light chain antibody (1:500 dilution, Bethyl) was used, and developed using anti-goat IgG (H+L)-HRP conjugated antibodies (1:500 dilution, Invitrogen).

Immunoprecipitations (IPs)

IPs were done essentially as previously described (Vazquez-Pianzola et al., 2011). 30 µl of protein-G Sepharose beads (Amersham) and 1 ml of embryo extracts were used per IP. Extracts were prepared from 0-20 h old embryos expressing a Chc::Myc fusion protein under a maternal Tubulin promoter. As a negative control, extracts were also prepared from wild-type embryos (OreR). For each IP, 1 ml of cell culture supernatant of monoclonal anti-BicD 1B11, anti-BicD 4C2, or anti-Myc 9E10 antibodies were bound to the beads. To IP TACC, a solution containing 2 µl of the polyclonal anti-TACC UT316 antibody (Kao and Megraw, 2009) diluted in 1 ml of PBS was used to bind to the protein-G beads. Beads were resuspended in 30 µl of sample buffer, and 7 to 15 µl per well was analyzed by Western blot.

Immunostainings

Immunostainings of embryos were done using the following primary antibodies: mouse anti-BicD (a mix of 1B11 and 4C2, 1:10 dilution), mouse anti-Myc 9E10 (dilution 1:5, DSHB), mouse anti-Flag (1:200, Sigma), mouse anti-V5 (1:200, Invitrogen), rabbit anti-Cnn (1:500 (Heuer et al., 1995)), rabbit anti Clc (1:500 (Heerssen et al., 2008)), mouse monoclonal anti-α-tubulin DM1A (1:500, Sigma), rabbit anti α-tubulin (1:500, Abcam), rabbit anti-GFP

(1:300, previously preabsorbed on embryos, Immunokontakt), rabbit anti D-TACC UT316 (1:1,000 (Kao and Megraw, 2009)), rabbit anti D-TACC (1:500 (Gergely et al., 2000)), rabbit anti-Msps (1:500 (Cullen et al., 1999)), mouse anti-Flag (1:200, Sigma, F3165) , rabbit anti CID (1:400 (Buster et al., 2013)), rabbit anti p-Histone H3 (S10) (1:200, Cell Signalling), mouse anti p-Histone H3 (1:200, Cell Signalling), rabbit anti BubR1 (1:2,000 (Logarinho et al., 2004)), and rabbit anti Mad2 (1/1,000 (Logarinho et al., 2004)). To detect the hb-deGRadFP construct, anti-llama IgG-heavy and light chain (1:500 dilution, Bethyl) was developed anti-goat Alexa Fluor 680 (H+L) (Ivitrogen).

Secondary antibodies used were Cy3-conjugated goat anti-mouse, DyLight 647-conjugated goat anti-mouse or anti-rabbit antibodies (Jackson Immunoresearch), A488-conjugated goat anti-rabbit (Molecular Probes), Oregon Green 488 conjugated goat anti-mouse (Molecular Probes), donkey anti-mouse AF488 (Molecular Probes), AF568 conjugated donkey anti-mouse, and AF488 conjugated donkey anti-rabbit A488 (Molecular Probes). Nuclei were visualized by staining DNA with 2.5 µg/ml Hoechst 33258 (Molecular Probes) for 40 minutes during the final wash or incubated overnight when early meiosis in embryos was analyzed. Control immunostainings using only secondary antibodies were performed to detect unspecific binding of the secondary antibodies. For co-localization studies, control samples using only one of the primary antibodies and both secondary antibodies were performed to detect bleed through to the other channel. When detecting tagged proteins, samples of wild-type specimens were used as a control for unspecific binding of the anti-tag antibody. Embryos were either fixed with 4% paraformaldehyde (PFA) or with methanol, as indicated. Methanol fixation was mainly used to preserve the cytoskeleton structure and or reduce the cytoplasmic levels in BicD staining. Methanol fixation was done as previously described (Kellogg et al., 1988). When antigens were not well preserved in methanol fixations (for example, this was observed for the Chc fusion proteins), fixation with 4% paraformaldehyde (PFA) was used. To detect endogenous BicD::GFP in ovaries, ovaries were fixed with 4% PFA. For preserving the endogenous Clc::GFP signal, embryos were hand-devitelinized and fixed in a mixture of Heptane saturated with PFA for 15 min. For preserving the Dj:mcherry and Chc::mCherry signal, the embryos were fixed with MetOH. Stage 14 oocytes for immunostainings were prepared as previously described (Radford and McKim, 2016).

Images were analyzed with a Leica TCS-SP8 confocal microscope. Most of the pictures represent z-stack maximal intensity projections along the frames. To detect the presence of Clc along the tandem meiosis spindles, Z-stack images were processed to correct for depth and bleaching in Image J. All stacks were processed the same way. First, a crop area corresponding to the spindle of the same size was cropped in each image. Channels were then split and subjected to corrections separately. Each channel was smooth with a median filter

radius of 1 to decrease the noise. The channel corresponding to the Clc staining had the most robust signal intensity loss through the sample´s depth. This channel was subject to bleach correction with a simple ratio fit to compensate for intensity attenuation in the image ´s deeper stacks. Channels corresponding to α-tubulin and DNA staining did not lose so much intensity with the sample´s depth. They were subjected to an attenuation correction using an ImageJ plugin already described (Biot et al., 2008). After intensity correction, the final image was created by merging the channels previously subjected to maximal intensity Z-stack projection.

In situ hybridization

For mRNA *in situ* hybridizations, RNA probes were prepared and *in situ* hybridization experiments were performed as previously described (Vazquez-Pianzola et al., 2017). To detect deGRadFP mRNA, a region of the deGradFP gene was first amplified by PCR with primers containing T3 and T7 promoter sequences, and the plasmid pUAS-Nslmb-vhhGFP4 as a template (Caussinus et al., 2011). Primer sequences were the following ones. The sense primer containing the T3 promoter was:
GGGGGGAATTAACCCTCACTAAAGGGAGAATGGATCAAGTCCAACTGGTGGAGT
and the antisense primer containing the T7 promoter was:
GGGGGGTAATACGACTCACTATAGGGAGATTAGCTGGAGACGGTGACCTGGGTG.
Antisense and sense probes were generated using T7 and T3 RNA polymerase, respectively. A sense probe was used to detect unspecific background.
DNA *in situs* to *Drosophila* chromosomes was done mainly according to (Dernburg, 2000). DNA oligos hybridizing to repetitive regions of the Y $(AATAC)_6$ and the 2nd chromosome $(AACAC)_7$ were ordered modified with Cy3 and Cy5 fluorophores at their 5' end, respectively, from Microsynth. The sequences were already described (Dernburg, 2000).The sequence used to detect the X chromosome by hybridizing to TTT- TCC-AAA-TTT-CGG-TCA-TCA-AAT-AAT-CAT recognizes the 359-bp satellite block on the *D. melanogaster* X chromosome as well as minor variants on Chromosome 3 was described by (Ferree and Barbash, 2009). A 5' end Cy5 fluorophore-labeled probe was used. Embryos were fixed with methanol for DNA *in situ* hybridizations. Probes were used at a final concentration of 5 ng/µl in hybridization buffer. The blocking buffer used (before adding the first antibody for detection of the desired proteins) was: 2x SSC, 0.5% BSA (molecular grade BSA from Biolabs or Acetylated BSA from Ambion), and Tween-20 at 0.1%. Donkey fluorescent-conjugated secondary antibodies were used as described in the immunofluorescence experiments.

RNAi in S2 cells

DNA fragments of BicD, Chc, and Clc, corresponding to the amplicons DRSC02006, DRSC20229, and DRSC42517 (https://www.flyrnai.org), were PCR amplified with sense and antisense primers containing T7 promoter sequences. LD43101 and GM02293 (BDGP resources) constructs containing *chc* and *Clc* cDNAs, respectively, and pBS-Bic-D plasmids were used as templates for the PCR. RNA was synthesized using 2 µg of PCR DNA template with the RNAMaxxTM high Yield transcription kit (Stratagene) following the manufacturer´s instructions. Transcription reactions were further subjected to DNase treatment and purification using the RNeasy Kit (Quiagen). $1x10^6$ S2 cells resuspended in 1ml of *Drosophila* Schneider's serum free medium containing 2 mM Glutamine were seeded into each well of a 6-well plate. 15 µg of the corresponding dsRNA was added to each well and incubated for 1 hour at RT. After that, 3 ml of Schneider medium containing 10% FCS and 50 µg ml^{-1} penicillin/streptomycin (complete medium) was added to each well. After one day, cells were resuspended and 1 ml of the resuspended cells was seeded into each well of a fresh 6-well plate. Finally, 0.5 ml of complete medium was added to each plate. 3-4 days after adding of dsRNA, cells were subjected to western blot or immunostaining. For immunostainings, the cells were resuspended and seeded on concavalin A-treated slides. Cells were allowed to settle shortly, then fixed with cold Methanol and subjected to immunostaining with the corresponding antibodies. For Western blots, the cells were washed once with cold 1x PBS, pelleted and resuspended in Hypotonic Buffer (10mM Hepes Ph 7.4, 10mM KAc, 1.5 mM MgAc, 2.5 mM DTT, 1% NP-40 plus protease inhibitors). Cells were incubated on ice for 15 min, vortexed for 10 seconds and centrifuge at 10.000 xg for 5 minutes at 4^0C. 1 to 3 µl of the supernatant was used to measure protein concentration using the Bio-Rad Protein assay solution. 5 µg of protein extract was loaded per well.

Yeast two hybrid experiments

Two hybrid plasmids containing the *Drosophila Egl* (Egl; CG4051) full-length (pEgl-AD and pEgl-BD), *BicD* full-length (pBicD-AD and pBicD-BD) and the *BicD* carboxy-terminal domain (CTD; amino acids 535–782) (pBicD(535–782)-BD and pBicD (535–782)-AD) were previously described (Rashpa et al., 2017). *D-TACC* (CG9765) full-length; and *Chc* (CG9012) full-length, a fragment containing amino acids 329-803, and another one bearing amino acids 329–542 were cloned into the pOAD and or pOBD2 vectors (Cagney et al., 2000) in-frame either with the activator domain (AD) or the DNA-binding domain (BD) sequence of GAL4, respectively, to create the "prey" plasmids, pD-TACC-AD, pChc-AD, pChc (329–803)-AD, and pChc(329–542)-AD, as well as the "bait" plasmids pChc-BD, pChc (329–803)-BD and pChc (329–542)-BD. To produce the constructs D-TACC-Ala and D-

TACC-Asp, D-TACC Ser863 was mutated to an alanine and aspartic acid codon, respectively, by site directed mutagenesis. Changes were verified by sequencing. Interactions between "bait" and "prey" proteins were detected following a yeast interaction-mating method using the strains PJ69-4a and PJ69-4alpha (Cagney et al., 2000). Diploid cells containing both bait and pray plasmids were grown in selective media –(Trp, Leu), spotted as serial dilutions on the auxotrophic medium –(Leu, Trp) and shown as growth control. Protein interactions were detected in serial dilutions by growing the diploid cells on the auxotrophic media –(Leu, Trp, adenine) or –(Leu, Trp, His) supplemented with the indicated amounts of 3-amino-1,2,4-triazole (3AT). Growth was scored after 4-5 days of growth at 30°C.

C. elegans strains, RNAi and imaging

N2, JDU233 (*H2B::mCherry;α-tubulin::GFP*), VJ512, *chc-1(tm2866)III/hT2[bli-4(e937) let-?(q782) qIs48](I;III)*. Feeding of RNAi was performed on NGM plates containing 1mM IPTG and carbenicillin using clones from the Ahringer RNAi library (Kamath et al., Nature 2003). For non-lethal phenotypes, the progeny was imaged after 60 hours of feeding of gravid adults at 20°C. For lethal phenotypes, L3/L4 larvae were transferred onto RNAi plates and incubated for 12 h at room temperature to obtain gravid adults. The empty vector L4440 was used as a control. Embryo dissections were performed as previously described (Bellanger et al., 2007), and embryos were imaged immediately on an agar pad using an AxioVision (Zeiss) microscope with an 100x NA 1.4 oil objective with a GFP and an mCherry filter set. One plane was acquired every 10 seconds using Visiview, and images were processed using ImageJ and Photoshop.

.

ACKNOWLEDGEMENTS

We thank S.L Bullock, C. Bazinet, J. Hirst**,** J. Raff, T.L. Melgraw, H. Ohkura, G.C. Rogers, C.E. Sunkel, Markus Affolter, Emmanuel Caussinus, the Bloomignton *Drosophila* Stock Center and the Developmental Studies Hybridoma Bank for antibodies, constructs and fly stocks. We thank FlyBase for the *Drosophila* genomic resources. We thank Andrew Swan for scientific advice on how to study female meiosis. This work was supported by the Swiss National Science Foundation and the Canton of Bern to B.S and an Equal Opportunity grant from the Phil.-Nat. faculty to P.V.P.

Competing interests. The authors declare no competing financial interests.

Author contributions. P.V.P., D. B., G.S., G. H., G. M. and D. H performed experiments. P.V.P., G. S., P.M. and G.H. analyzed data. P.V. P. and B.S. conceived the studies. G.S. and

P. M. contributed on writing the results of the *C. elegans* experiments. P.V.P and B.S. wrote the manuscript.

REFERENCES

Barros, T. P., Kinoshita, K., Hyman, A. A. and Raff, J. W. (2005). Aurora A activates D-TACC-Msps complexes exclusively at centrosomes to stabilize centrosomal microtubules. *J Cell Biol* **170**, 1039–1046.

Basto, R., Scaerou, F., Mische, S., Wojcik, E., Lefebvre, C., Gomes, R., Hays, T. and Karess, R. (2004). In vivo dynamics of the rough deal checkpoint protein during *Drosophila* mitosis. *Curr. Biol.* **14**, 56–61.

Bazinet, C., Katzen, A. L., Morgan, M., Mahowald, A. P. and Lemmon, S. K. (1993). The Drosophila clathrin heavy chain gene: clathrin function is essential in a multicellular organism. *Genetics* **134**, 1119–1134.

Bellanger, J.-M., Carter, J. C., Phillips, J. B., Canard, C., Bowerman, B. and Gönczy, P. (2007). ZYG-9, TAC-1 and ZYG-8 together ensure correct microtubule function throughout the cell cycle of *C. elegans* embryos. *Journal of Cell Science* **120**, 2963–2973.

Berleth, T., Burri, M., Thoma, G., Bopp, D., Richstein, S., Frigerio, G., Noll, M. and Nüsslein-Volhard, C. (1988). The role of localization of *bicoid* RNA in organizing the anterior pattern of the *Drosophila* embryo. *EMBO J.* **7**, 1749–1756.

Biot E, Crowell E, Höfte H, Maurin Y, Vernhettes S & Andrey P. (2008). A new filter for spot extraction in *N*-dimensional biological imaging. In *Fifth IEEE International Symposium on Biomedical Imaging (ISBI'08): From Nano to Macro*, pp. 975-978.

Booth, D. G., Hood, F. E., Prior, I. A. and Royle, S. J. (2011). A TACC3/ch-TOG/clathrin complex stabilises kinetochore fibres by inter-microtubule bridging. *EMBO J.* **30**, 906–919.

Brodsky, F. M. (2012). Diversity of clathrin function: new tricks for an old protein. *Annu. Rev. Cell Dev. Biol.* **28**, 309–336.

Bullock, S. L. and Ish-Horowicz, D. (2001). Conserved signals and machinery for RNA transport in *Drosophila* oogenesis and embryogenesis. *Nature* **414**, 611–616.

Buster, D. W., Daniel, S. G., Nguyen, H. Q., Windler, S. L., Skwarek, L. C., Peterson, M., Roberts, M., Meserve, J. H., Hartl, T., Klebba, J. E., et al. (2013). SCFSlimb ubiquitin ligase suppresses condensin II-mediated nuclear reorganization by degrading Cap-H2. *J Cell Biol* **201**, 49–63.

Cagney, G., Uetz, P. and Fields, S. (2000). High-throughput screening for protein-protein interactions using two-hybrid assay. *Meth. Enzymol.* **328**, 3–14.

Caussinus, E., Kanca, O. and Affolter, M. (2011). Fluorescent fusion protein knockout mediated by anti-GFP nanobody. *Nature Publishing Group* **19**, 117–121.

Conde, C., Osswald, M., Barbosa, J., Moutinho-Santos, T., Pinheiro, D., Guimarães, S., Matos, I., Maiato, H. and Sunkel, C. E. (2013). *Drosophila* Polo regulates the spindle

1034 assembly checkpoint through Mps1-dependent BubR1 phosphorylation. *EMBO J.* **32**,
1035 1761–1777.

1036 **Cullen, C. F. and Ohkura, H.** (2001). Msps protein is localized to acentrosomal poles to
1037 ensure bipolarity of *Drosophila* meiotic spindles. *Nat. Cell Biol.* **3**, 637–642.

1038 **Cullen, C. F., Deák, P., Glover, D. M. and Ohkura, H.** (1999). *mini spindles*: A gene
1039 encoding a conserved microtubule-associated protein required for the integrity of the
1040 mitotic spindle in *Drosophila*. *J Cell Biol* **146**, 1005–1018.

1041 **De Renzis, S., Elemento, O., Tavazoie, S. and Wieschaus, E. F.** (2007). Unmasking
1042 activation of the zygotic genome using chromosomal deletions in the *Drosophila*
1043 embryo. *PLoS Biol.* **5**, e117.

1044 **Défachelles, L., Hainline, S. G., Menant, A., Lee, L. A. and Karess, R. E.** (2015). A
1045 maternal effect *rough deal* mutation suggests that multiple pathways regulate *Drosophila*
1046 RZZ kinetochore recruitment. *Journal of Cell Science* **128**, 1204–1216.

1047 **Dernburg A. F.** (2000) *In Situ* hybridization to somatic chromosomes. In: Drosophila
1048 Protocols (ed. W. Sullivan, M. Ashburner and R. S. Hawley), pp. 24–55. Cold Spring
1049 Harbor, New York, USA: Cold Spring Harbor Laboratory Press.
1050
1051 **Dienstbier, M., Boehl, F., Li, X. and Bullock, S. L.** (2009). Egalitarian is a selective RNA-
1052 binding protein linking mRNA localization signals to the dynein motor. *Genes Dev.* **23**,
1053 1546–1558.
1054
1055 **Driever, W. and Nüsslein-Volhard, C.** (1988). A gradient of bicoid protein in *Drosophila*
1056 embryos. *Cell* **54**, 83–93.

1057 **Edgar, B. A. and Schubiger, G.** (1986). Parameters controlling transcriptional activation
1058 during early *Drosophila* development. *Cell* **44**, 871–877.

1059 **Espeut, J., Lara-Gonzalez, P., Sassine, M., Shiau, A. K., Desai, A. and Abrieu, A.** (2015).
1060 Natural Loss of Mps1 Kinase in Nematodes Uncovers a Role for Polo-like Kinase 1 in
1061 Spindle Checkpoint Initiation. *Cell Rep* **12**, 58–65.

1062 **Ferree, P. M. and Barbash, D. A.** (2009). Species-specific heterochromatin prevents mitotic
1063 chromosome segregation to cause hybrid lethality in *Drosophila*. *PLoS Biol.* **7**,
1064 e1000234.

1065 **Fischer, M. G., Heeger, S., Häcker, U. and Lehner, C. F.** (2004). The mitotic arrest in
1066 response to hypoxia and of polar bodies during early embryogenesis requires *Drosophila*
1067 *Mps1*. *Curr. Biol.* **14**, 2019–2024.

1068 **Foraker, A. B., Camus, S. M., Evans, T. M., Majeed, S. R., Chen, C.-Y., Taner, S. B.,**
1069 **Corrêa, I. R., Doxsey, S. J. and Brodsky, F. M.** (2012). Clathrin promotes centrosome
1070 integrity in early mitosis through stabilization of centrosomal ch-TOG. *J Cell Biol* **198**,
1071 591–605.

1072 **Fu, W., Tao, W., Zheng, P., Fu, J., Bian, M., Jiang, Q., Clarke, P. R. and Zhang, C.**
1073 (2010). Clathrin recruits phosphorylated TACC3 to spindle poles for bipolar spindle
1074 assembly and chromosome alignment. *Journal of Cell Science* **123**, 3645–3651.

1075 **Fumoto, K., Hoogenraad, C. C. and Kikuchi, A.** (2006). GSK-3beta-regulated interaction
1076 of BICD with dynein is involved in microtubule anchorage at centrosome. *EMBO J.* **25**,

5670–5682.

Gergely, F., Kidd, D., Jeffers, K., Wakefield, J. G. and Raff, J. W. (2000). D-TACC: a novel centrosomal protein required for normal spindle function in the early *Drosophila* embryo. *EMBO J.* **19**, 241–252.

Gönczy, P., Pichler, S., Kirkham, M. and Hyman, A. A. (1999). Cytoplasmic dynein is required for distinct aspects of MTOC positioning, including centrosome separation, in the one cell stage *Caenorhabditis elegans* embryo. *J Cell Biol* **147**, 135–150.

Gutiérrez-Caballero, C., Burgess, S. G., Bayliss, R. and Royle, S. J. (2015). TACC3-ch-TOG track the growing tips of microtubules independently of clathrin and Aurora-A phosphorylation. *Biol Open* **4**, 170–179.

Heerssen, H., Fetter, R. D. and Davis, G. W. (2008). Clathrin dependence of synaptic-vesicle formation at the *Drosophila* neuromuscular junction. *Curr. Biol.* **18**, 401–409.

Heuer, J. G., Li, K. and Kaufman, T. C. (1995). The *Drosophila* homeotic target gene *centrosomin (cnn)* encodes a novel centrosomal protein with leucine zippers and maps to a genomic region required for midgut morphogenesis. *Development* **121**, 3861–3876.

Hirst, J., Sahlender, D. A., Choma, M., Sinka, R., Harbour, M. E., Parkinson, M. and Robinson, M. S. (2009). Spatial and functional relationship of GGAs and AP-1 in Drosophila and HeLa cells. *Traffic* **10**, 1696–1710.

Hoogenraad, C. C. and Akhmanova, A. (2016). Bicaudal D Family of Motor Adaptors: Linking Dynein Motility to Cargo Binding. *Trends Cell Biol.* **26**, 327–340.

Howell, B. J., McEwen, B. F., Canman, J. C., Hoffman, D. B., Farrar, E. M., Rieder, C. L. and Salmon, E. D. (2001). Cytoplasmic dynein/dynactin drives kinetochore protein transport to the spindle poles and has a role in mitotic spindle checkpoint inactivation. *J Cell Biol* **155**, 1159–1172.

Ikeda, M. and Tanaka, K. (2017). Plk1 bound to Bub1 contributes to spindle assembly checkpoint activity during mitosis. *Sci Rep* **7**, 8794–15.

Jackson, J. R., Patrick, D. R., Dar, M. M. and Huang, P. S. (2007). Targeted anti-mitotic therapies: can we improve on tubulin agents? *Nat. Rev. Cancer* **7**, 107–117.

Kamath, R. S. and Ahringer, J. (2003). Genome-wide RNAi screening in Caenorhabditis elegans. *Methods* **30**, 313–321.

Kao, L.-R. and Megraw, T. L. (2009). Centrocortin Cooperates with Centrosomin to Organize *Drosophila* Embryonic Cleavage Furrows. *Curr. Biol.* **19**, 937–942.

Kasprowicz, J., Kuenen, S., Miskiewicz, K., Habets, R. L. P., Smitz, L. and Verstreken, P. (2008). Inactivation of clathrin heavy chain inhibits synaptic recycling but allows bulk membrane uptake. *J Cell Biol* **182**, 1007–1016.

Kellogg, D. R., Mitchison, T. J. and Alberts, B. M. (1988). Behaviour of microtubules and actin filaments in living *Drosophila* embryos. *Development* **103**, 675–686.

Kleist, von, L., Stahlschmidt, W., Bulut, H., Gromova, K., Puchkov, D., Robertson, M. J., MacGregor, K. A., Tomilin, N., Tomlin, N., Pechstein, A., et al. (2011). Role of the clathrin terminal domain in regulating coated pit dynamics revealed by small molecule

1117 inhibition. *Cell* **146**, 471–484.

1118 **Koch, R., Ledermann, R., Urwyler, O., Heller, M. and Suter, B.** (2009). Systematic
1119 functional analysis of Bicaudal-D serine phosphorylation and intragenic suppression of a
1120 female sterile allele of *BicD*. *PLoS ONE* **4**, e4552.

1121 **Laband, K., Lacroix, B., Edwards, F., Canman, J. C. and Dumont, J.** (2018). Live
1122 imaging of *C. elegans* oocytes and early embryos. *Methods Cell Biol.* **145**, 217–236.

1123 **Lee, M. J., Gergely, F., Jeffers, K., Peak-Chew, S. Y. and Raff, J. W.** (2001).
1124 Msps/XMAP215 interacts with the centrosomal protein D-TACC to regulate microtubule
1125 behaviour. *Nat. Cell Biol.* **3**, 643–649.

1126 **Levine, M. S. and Holland, A. J.** (2018). The impact of mitotic errors on cell proliferation
1127 and tumorigenesis. *Genes Dev.* **32**, 620–638.

1128 **Li, X., Kuromi, H., Briggs, L., Green, D. B., Rocha, J. A. O. J., Sweeney, S. T. and**
1129 **Bullock, S. L.** (2010). Bicaudal-D binds clathrin heavy chain to promote its transport and
1130 augments synaptic vesicle recycling. *EMBO J.* **29**, 992–1006.

1131 **Lin, C.-H., Hu, C.-K. and Shih, H.-M.** (2010). Clathrin heavy chain mediates TACC3
1132 targeting to mitotic spindles to ensure spindle stability. *J Cell Biol* **189**, 1097–1105.

1133 **Logarinho, E., Bousbaa, H., Dias, J. M., Lopes, C., Amorim, I., Antunes-Martins, A. and**
1134 **Sunkel, C. E.** (2004). Different spindle checkpoint proteins monitor microtubule
1135 attachment and tension at kinetochores in *Drosophila* cells. *Journal of Cell Science* **117**,
1136 1757–1771.

1137 **Lu, A., Zhou, C.-J., Wang, D.-H., Han, Z., Kong, X.-W., Ma, Y.-Z., Yun, Z.-Z. and**
1138 **Liang, C.-G.** (2017). Cytoskeleton-associated protein 5 and clathrin heavy chain binding
1139 regulates spindle assembly in mouse oocytes. *Oncotarget* **8**, 17491–17503.

1140 **Lucaj, C. M., Evans, M. F., Nwagbara, B. U., Ebbert, P. T., Baker, C. C., Volk, J. G.,**
1141 **Francl, A. F., Ruvolo, S. P. and Lowery, L. A.** (2015). *Xenopus* TACC1 is a
1142 microtubule plus-end tracking protein that can regulate microtubule dynamics during
1143 embryonic development. *Cytoskeleton (Hoboken)* **72**, 225–234.

1144 **Mach, J. M. and Lehmann, R.** (1997). An Egalitarian-BicaudalD complex is essential for
1145 oocyte specification and axis determination in *Drosophila*. *Genes Dev.* **11**, 423–435.

1146 **Margolis, J. S., Borowsky, M., Shim, C. W. and Posakony, J. W.** (1994). A small region
1147 surrounding the distal promoter of the *hunchback* gene directs maternal expression. *Dev.*
1148 *Biol.* **163**, 381–388.

1149 **Maro, B., Johnson, M. H., Pickering, S. J. and Louvard, D.** (1985). Changes in the
1150 distribution of membranous organelles during mouse early development. *J Embryol Exp*
1151 *Morphol* **90**, 287–309.

1152 **Marston, A. L. and Wassmann, K.** (2017). Multiple Duties for Spindle Assembly
1153 Checkpoint Kinases in Meiosis. *Front Cell Dev Biol* **5**, 109.

1154 **Mirouse, V., Formstecher, E. and Couderc, J. L.** (2006). Interaction between Polo and
1155 BicD proteins links oocyte determination and meiosis control in *Drosophila*.
1156 *Development* **133**, 4005–4013.

Nag, R. N., Niggli, S., Sousa-Guimarães, S., Vazquez-Pianzola, P. and Suter, B. (2018). *Mms19* is a mitotic gene that permits Cdk7 to be fully active as a Cdk-activating kinase. *Development* **145**, dev156802.

Nwagbara, B. U., Faris, A. E., Bearce, E. A., Erdogan, B., Ebbert, P. T., Evans, M. F., Rutherford, E. L., Enzenbacher, T. B. and Lowery, L. A. (2014). TACC3 is a microtubule plus end-tracking protein that promotes axon elongation and also regulates microtubule plus end dynamics in multiple embryonic cell types. *Mol. Biol. Cell* **25**, 3350–3362.

Paré, C. and Suter, B. (2000). Subcellular localization of Bic-D::GFP is linked to an asymmetric oocyte nucleus. *Journal of Cell Science* **113 (Pt 12)**, 2119–2127.

Payne, C., Rawe, V., Ramalho-Santos, J., Simerly, C. and Schatten, G. (2003). Preferentially localized dynein and perinuclear dynactin associate with nuclear pore complex proteins to mediate genomic union during mammalian fertilization. *Journal of Cell Science* **116**, 4727–4738.

Pérez-Mongiovi, D., Malmanche, N., Bousbaa, H. and Sunkel, C. (2005). Maternal expression of the checkpoint protein BubR1 is required for synchrony of syncytial nuclear divisions and polar body arrest in *Drosophila melanogaster*. *Development* **132**, 4509–4520.

Radford, S. J. and McKim, K. S. (2016). Techniques for Imaging Prometaphase and Metaphase of Meiosis I in Fixed *Drosophila* Oocytes. *J Vis Exp* e54666.

Ran, B., Bopp, R. and Suter, B. (1994). Null alleles reveal novel requirements for *Bic-D* during *Drosophila* oogenesis and zygotic development. *Development* **120**, 1233–1242.

Rashpa, R., Vazquez-Pianzola, P., Colombo, M., Hernandez, G., Beuchle, D., Berger, F., Peischl, S., Bruggmann, R. and Suter, B. (2017). *Cbp80* is needed for the expression of piRNA components and piRNAs. *PLoS ONE* **12**, e0181743.

Rieder, C. L. and Maiato, H. (2004). Stuck in division or passing through: what happens when cells cannot satisfy the spindle assembly checkpoint. *Dev. Cell* **7**, 637–651.

Riparbelli, M. G. and Callaini, G. (2005). The meiotic spindle of the *Drosophila* oocyte: the role of centrosomin and the central aster. *Journal of Cell Science* **118**, 2827–2836.

Riparbelli, M. G., Callaini, G. and Glover, D. M. (2000). Failure of pronuclear migration and repeated divisions of polar body nuclei associated with MTOC defects in *polo* eggs of *Drosophila*. *Journal of Cell Science* **113 (Pt 18)**, 3341–3350.

Royle, S. J. (2012). The role of clathrin in mitotic spindle organisation. *Journal of Cell Science* **125**, 19–28.

Royle, S. J. and Lagnado, L. (2006). Trimerisation is important for the function of clathrin at the mitotic spindle. *Journal of Cell Science* **119**, 4071–4078.

Royle, S. J., Bright, N. A. and Lagnado, L. (2005). Clathrin is required for the function of the mitotic spindle. *Nature* **434**, 1152–1157.

Rutherford, E. L., Carandang, L., Ebbert, P. T., Mills, A. N., Bowers, J. T. and Lowery, L. A. (2016). *Xenopus* TACC2 is a microtubule plus end-tracking protein that can promote microtubule polymerization during embryonic development. *Mol. Biol. Cell* **27**,

3013–3020.

Sallés, F. J., Lieberfarb, M. E., Wreden, C., Gergen, J. P. and Strickland, S. (1994). Coordinate initiation of *Drosophila* development by regulated polyadenylation of maternal messenger RNAs. *Science* **266**, 1996–1999.

Santel, A., Winhauer, T., Blümer, N. and Renkawitz-Pohl, R. (1997). The *Drosophila don juan (dj)* gene encodes a novel sperm specific protein component characterized by an unusual domain of a repetitive amino acid motif. *Mech. Dev.* **64**, 19–30.

Sawicka, A. and Seiser, C. (2012). Histone H3 phosphorylation - a versatile chromatin modification for different occasions. *Biochimie* **94**, 2193–2201.

Schubert, von, C., Cubizolles, F., Bracher, J. M., Sliedrecht, T., Kops, G. J. P. L. and Nigg, E. A. (2015). Plk1 and Mps1 Cooperatively Regulate the Spindle Assembly Checkpoint in Human Cells. *Cell Rep* **12**, 66–78.

Schulz, C. and Tautz, D. (1995). Zygotic *caudal* regulation by *hunchback* and its role in abdominal segment formation of the *Drosophila* embryo. *Development* **121**, 1023–1028.

Smith, C. M., Haucke, V., McCluskey, A., Robinson, P. J. and Chircop, M. (2013). Inhibition of clathrin by pitstop 2 activates the spindle assembly checkpoint and induces cell death in dividing HeLa cancer cells. *Mol. Cancer* **12**, 4–15.

So, C., Seres, K. B., Steyer, A. M., Mönnich, E., Clift, D., Pejkovska, A., Möbius, W. and Schuh, M. (2019). A liquid-like spindle domain promotes acentrosomal spindle assembly in mammalian oocytes. *Science* **364**, eaat9557.

Sokac, A. M. and Wieschaus, E. (2008). Local actin-dependent endocytosis is zygotically controlled to initiate Drosophila cellularization. *Dev. Cell* **14**, 775–786.

Suter, B. and Steward, R. (1991). Requirement for phosphorylation and localization of the Bicaudal-D protein in *Drosophila* oocyte differentiation. *Cell* **67**, 917–926.

Suter, B., Romberg, L. M. and Steward, R. (1989). *Bicaudal-D*, a *Drosophila* gene involved in developmental asymmetry: localized transcript accumulation in ovaries and sequence similarity to myosin heavy chain tail domains. *Genes Dev.* **3**, 1957–1968.

Swan, A. and Suter, B. (1996). Role of *Bicaudal-D* in patterning the *Drosophila* egg chamber in mid-oogenesis. *Development* **122**, 3577–3586.

Tahara, H., Yokota, E., Igarashi, H., Orii, H., Yao, M., Sonobe, S., Hashimoto, T., Hussey, P. J. and Shimmen, T. (2007). Clathrin is involved in organization of mitotic spindle and phragmoplast as well as in endocytosis in tobacco cell cultures. *Protoplasma* **230**, 1–11.

Vazquez-Pianzola, P. and Suter, B. (2012). Conservation of the RNA Transport Machineries and Their Coupling to Translation Control across Eukaryotes. *Comp. Funct. Genomics* **2012**, 287852–13.

Vazquez-Pianzola P., Suter B., Hernández G. (2016) Evolution of the Molecules Coupling mRNA Transport with Translational Control in Metazoans. In: Evolution of the Protein Synthesis Machinery and Its Regulation (ed. G.Hernández R. Jagus), pp. 531-546. New York, USA: Springer, Cham.

Vazquez-Pianzola, P., Adam, J., Haldemann, D., Hain, D., Urlaub, H. and Suter, B. (2014). Clathrin heavy chain plays multiple roles in polarizing the *Drosophila* oocyte downstream of *Bic-D*. *Development* **141**, 1915–1926.

Vazquez-Pianzola, P., Schaller, B., Colombo, M., Beuchle, D., Neuenschwander, S., Marcil, A., Bruggmann, R. and Suter, B. (2017). The mRNA transportome of the BicD/Egl transport machinery. *RNA Biol* **14**, 73–89.

Vazquez-Pianzola, P., Urlaub, H. and Suter, B. (2011). Pabp binds to the *osk* 3'UTR and specifically contributes to *osk* mRNA stability and oocyte accumulation. *Dev. Biol.* **357**, 404–418.

Wharton, R. P. and Struhl, G. (1989). Structure of the *Drosophila* BicaudalD protein and its role in localizing the posterior determinant *nanos*. *Cell* **59**, 881–892.

Wojcik, E., Basto, R., Serr, M., Scaërou, F., Karess, R. and Hays, T. (2001). Kinetochore dynein: its dynamics and role in the transport of the Rough deal checkpoint protein. *Nat. Cell Biol.* **3**, 1001–1007.

Yamauchi, T., Ishidao, T., Nomura, T., Shinagawa, T., Tanaka, Y., Yonemura, S. and Ishii, S. (2008). A B-Myb complex containing clathrin and filamin is required for mitotic spindle function. *EMBO J.* **27**, 1852–1862.

FIGURE LEGENDS

Figure 1. Dynamic localization of BicD and Chc during the embryonic cell cycle with enrichment at the mitotic spindles and centrosomes. (A) Methanol fixed wild-type embryos were stained for BicD (red) and Cnn (green). BicD colocalized with the pericentrosomal (PCM) Cnn throughout the cell cycle. BicD it also present at the mitotic spindles where it is clearly detected in metaphase. Scale bars represent 5 μm **(B)** BicD::GFP expressing embryos were stained using anti-GFP (green) and anti-α-tubulin (red) antibodies. The BicD::GFP fusion protein was also detected at centrosomes and spindles. Scale bars represent 5 μm. **(C)** Embryos expressing a V5-tagged version of Chc were stained with anti-V5 (red) and anti-Cnn (green) antibodies. During interphase and prophase (right panels), the Chc::V5 fusion protein localized near the membranes that have started to invaginate and also to the centrosomes as seen by its co-localization with Cnn. In metaphase (left panels), Chc::V5 can be clearly detected at the mitotic spindle and the centrosomes**. (D)** Embryos expressing a Chc::mCherry were subject to live imaging to detect the dynamic movement of Chc during the cell cycle. Scale bar represent 10 μm. Embryos in A-C were also stained with Hoechst (blue) to visualize the DNA.

Figure 2. *hb-deGradFP* degrades BicD::GFP specifically during embryogenesis causing early embryonic developmental arrest. (A) Scheme depicting the construct expressed in flies (not drawn to scale). **(B)** RNA *in situ* hybridization to detect the expression and localization of the mRNA expressed from the *deGradFP* construct. A digoxigenin-labeled probe complementary to the *VhhGFP4* region of the *deGradFP* construct was used. Due to the presence of the *bcd* 3' UTR, the mRNA is enriched in the anterior region of the embryos from early embryogenesis on. **(C)** Expression of the lamma anti-GFP nanobody expressed from the *deGradFP* construct was detected by immunofluorescence using anti-lamma IgG antibodies. The *deGradFP* construct was weakly and ubiquitously expressed in embryos from mothers with the *deGradFP* transgene, but not in control embryos. DNA (blue) was stained with Hoechst. Wild-type embryos were used as negative control in B and C. **(D)** Percentage of embryos that hatched as larvae. Eggs were laid by mothers of the depicted genotypes mated to wild-type males. **(E)** Embryos laid by the same mothers as in D were collected and aged to obtain 2 to 5h old embryos. After fixing, they were stained with Hoechst and α-tubulin to visualize the progression of their development. The percentage of developed embryos was determined for each maternal genotype. **(F-I)** Control females (*BicD::GFP,* $BicD^{null}$) and $BicD^{hb\text{-}deGradFP}$ females were used to analyzed the effect of knocking down BicD using the *hb-deGradFP* construct. After mating them with wild type males, ovaries of the mothers and their embryos were used for IF and western blot analysis. **(F)** BicD::GFP (green) levels, detected by visualization of endogenous GFP signal, were not affected in $BicD^{hb\text{-}deGradFP}$ ovaries. Ovaries were also stained with Hoechst to visualize the DNA. Scale bars are 15 µm. **(G)** Ubiquitously degradation of the BicD::GFP protein was detected in $BicD^{hb\text{-}deGradFP}$ embryos by Immunofluorescence using anti-GFP antibodies (green). Embryos were also stained with anti-α-tubulin antibodies (red) to analyze their development. Scale bars are 100 µm. **(H-I)** Western blots to detect the expression of BicD::GFP and the deGradFP construct in ovaries **(H)** and 0-2h old embryos **(I)** using anti-GFP and anti-lamma IgG antibodies, respectively. α-tubulin was used as loading control and increasing amounts of cytoplasmic extracts were loaded onto the gel for each sample. Degradation of BicD::GFP fusion protein was observed in $BicD^{hb\text{-}deGradFP}$ embryos (I), but not in ovaries of the same mothers (H). High expression of the deGradFP VhhGFP nanobody was detected in $BicD^{hb\text{-}deGradFP}$ embryos by Western blots. deGradFP VhhGFP was also detected at low levels in ovaries, probably due to egg activation and release from metaphase I arrest due to physical egg activation during the dissection (see text for details).

Figure 3. Fertilized *BicD*$^{hb\text{-}deGradFP}$ embryos arresting at the start of embryogenesis with abnormal spindle figures and over-replicated polar bodies fail to perform pronuclear fusion. (A-C) Females of the depicted genotypes were crossed to wild type males. 20-30 min old embryos were collected, stained with anti-α-tubulin antibodies to detect the spindles (red), anti-Cnn to mark the centrosomes (green) and Hoechst to visualize the DNA (blue). Embryos were classified as follows: normal development when they went through the 2nd mitotic division (showing the presence of four or more zygotic nuclei inside the embryo; arrested with centrosomes**,** when embryos showed one or more inner abnormal spindles with centrosomes or free centrosomes positive for Cnn staining; arrested, acentrosomal, when the embryos had one or more acentrosomal spindle that was negative for Cnn and did not form the rosette-like structure that is typical for meiosis that had proceeded normally. Normal completion of meiosis II takes place even in the absence of fertilization when egg activation is triggered as the egg passes through the oviduct and ends with the formation of 4 polar bodies that arrange in rosette-like structures (mainly fused into a single one) at the surface at the embryonic surface and no internal nuclei. We found that the proportion of eggs that looked like they have normally completed meiosis II in the absence of fertilization was similar for the different genotypes. However, *BicD*$^{hb\text{-}deGradFP}$ mothers laid a higher proportion of embryos classified as arrested with centrosomes and arrested, acentrosomal. Two independent embryo collections (n1 and n2) were analyzed. The percentage of embryos observed with the indicated phenotypes is depicted in the plot **(A).** Error bars show the SD. For *BicD::GFP, BicD*^{null}*/BicD::GFP, BicD*^{null} *n1=84, n2=82* , for *BicD::GFP, BicD*^{null}*/ + ; deGradFP /deGradFP n1=55, n2=70* and *BicD*$^{hb\text{-}deGradFP}$ *n1=42, n2=63* were analyzed. Examples of the observed phenotypes are shown in **B-C**. **(B)** Control embryo (from a *BicD::GFP, BicD*^{null} homozygous mother) going through normal zygotic divisions**. (C) (a)** *BicD*$^{hb\text{-}deGradFP}$ embryo arrested in development and classified as "arrested with centrosomes". Upper left panel overview of the spindles present in the embryo (stained for α-tubulin). Panels on the right show magnified views of the corresponding spindles marked with boxes observed in this embryo. **(b)** Overview of a *BicD*$^{hb\text{-}deGradFP}$ embryo classified as "arrested, acentrosomal" and magnified view of the individual spindle-like structures marked with yellow boxes. Scale bars represent 30 μm for entire embryo pictures and 10 μm for the magnified spindles. **(D-E)** DNA *in situ* hybridization with probes detecting the presence of X (white) and Y (red) chromosomes. Mothers of the indicated phenotype were crossed to wild-type males. Embryos were also stained for α-tubulin (green) and DNA (blue). Both embryos contain a sperm tail (arrows). **(D)** Example of a male embryo in the 2nd mitotic metaphase laid by a wild-type control mother. Both zygotic nuclei were detected by the Y probe (Y is derived from the father) and one the X chromosomal probe (X derived from the mother). Magnified view of

one of the two mitotic spindles is shown in 2. The polar bodies have fused into a single rosette, that contains the 3 remaining X chromosomes from the mother (magnified in 1). **(E)** Example of a male embryo derived from a *BicD*$^{hb\text{-}deGradFP}$ mother. This embryo is arrested showing acentrosomal like spindles but containing free centrosomes (arrowheads). The paternal pro-nucleus is in metaphase and is marked with two signals for the Y chromosome (magnified in 2), indicating that it had undergone one round of replication. The remaining nuclei are marked by several dots of the X-chromosome, suggesting that they are over-replicated polar bodies (or possibly polar bodies with fragmentated DNA) that did not fuse (magnified in 1 and 3). Images are z-stack projections through the nuclei. Scales bars represent 30 µm in all embryo pictures and 5 µm in the insets.

Figure 4. Female meiotic products fail to arrest in metaphase and undergo extra rounds of replication in unfertilized *BicD*$^{hb\text{-}deGradFP}$ eggs.

(A) Females of the depicted genotypes were crossed to XO males to obtain unfertilized eggs. 0-1 h old eggs were stained for α-tubulin (red) and DNA (blue). They were classified as follows: eggs that seemed to have completed meiosis normally (showing the typical up to four rosette like structures that normally fuse into one single rosette); eggs showing a normal metaphase I tandem spindle; eggs presenting rosette like structures (1 to 2) plus (1 to 2) spindles (probably representing normal meiosis intermediate products); eggs with a big DNA blob surrounded by a star of microtubules (MT); eggs containing one big spindle; eggs containing several acentrosomal like spindles and eggs with other defects. The percentage of eggs showing the described phenotypes was scored. Most control eggs (laid by wild type, *BicD::GFP, BicD*^{null} or *BicD::GFP, BicD*^{null}*/ + ; hb-deGradFP* mothers) completed meiosis normally. In contrast, *BicD*$^{hb\text{-}deGradFP}$ mothers laid mainly eggs with several acentrosomal spindles and to a lesser extent eggs containing one big spindle. Error bars show the SD of three to four independent egg collections (n1 to n4). For *Wild type* n1= 145 n2=95 n3=67, for *BicD::GFP, BicD*^{null}*/BicD::GFP* n1=92 n2=72 n3=147, for *BicD*^{null}, *BicD::GFP/ +; deGradFP /deGradFP* n1=68 n2=46 n3= 69 n4=67, for *BicD*$^{hb\text{-}deGradFP}$ *n1=29 n2=45 n3=32* were scored. **(B-C)** Eggs from the same parents as in A) were subjected to DNA *in situ* hybridization with a probe to detect the X chromosome (white), α-tubulin (red) and DNA (Blue). **(B)** Most eggs in control samples (pictures are from eggs laid by *BicD::GFP, BicD*^{null} homozygous rescued females) show normal completion of meiosis. Magnified pictures of the meiotic products for two different control embryos are shown (b, b'). In b, the polar bodies have fused into a single rosette. In b', the two rosette like structures contain 1 and 3 chromosomes, respectively. The polar bodies in each egg contain a total of four X chromosomes, corresponding to the four meiotic products that are produced after normal

completion of meiosis II. **(C)** (c) Example of a *BicD*$^{hb\text{-}deGradFP}$ egg showing the presence of a single nucleus with an abnormal rosette like structure, partially de-condensed chromosomes and with many dotted X chromosomal signals. (c') Sows a *BicD*$^{hb\text{-}deGradFP}$ egg that has more than four meiotic products. In every spindle many dotted X chromosomal signals can be seen on the accompanying magnified pictures (1 and 2). In c'2, the female meiotic products are in late anaphase and they have clearly undergone additional replications. Images are z-stack projections though the eggs. Scales bars represent 5 μm. **(D-E)** Wild type (control) and *BicD*$^{hb\text{-}deGradFP}$ females were crossed to XO males to obtain unfertilized eggs. 0-1 h old eggs were collected. **(D)** Eggs were stained for CID (green, marking centromeres), PH3 (red) and DNA (blue). 100% (12/12 confocal images) of the single fused rosette nuclei in control eggs, showed a strong PH3 staining along the entire chromosomes. In contrast, 90,9 % (10/11 of the analyzed confocal pictures) of the single fused rosette-like structures in *BicD*$^{hb\text{-}deGradFP}$ eggs showed a PH3 staining signal that was not localized along the entire chromosomes but was only enriched at the pericentromeric region. 86% (6/7 confocal images) of the single fused rosette-like nuclei in control eggs showed a normal CID staining. In contrast, 63.7 % (7/11 of the analyzed confocal pictures) of the single rosette-like structures in *BicD*$^{hb\text{-}deGradFP}$ eggs showed an increase number of CID-positive dots. **(E)** Eggs were stained for α-tubulin (red), PH3 (green) and DNA (blue). Nuclei in Ec labeled 1-3 are the magnified nuclei observed in the embryo depicted in Ec'. Images are z-stack projections though the nuclei. Scale bars represent 5 μm, except in Ec' where scale bar represents 10 μm.

Figure 5. SAC components BubR1 and Mad2 are not properly recruited to female meiotic products in *BicD*$^{hb\text{-}deGradFP}$ eggs. Control females (either wild type or rescued *BicD::GFP, BicD*^{null}) (a), and *BicD*$^{hb\text{-}deGradFP}$ females (b-d) were crossed to XO males to obtain unfertilized eggs. 0-1 h old eggs were collected. Eggs were stained for α-tubulin (red), DNA (blue) and BubR1 **(A)** or Mad2 **(B)** (green signals). (**A) a)** The meiotic products fused into a single rosette in a wild-type control egg showed BubR1 staining at the kinetochores. (**A) b)** Example of *BicD*$^{hb\text{-}deGradFP}$ egg containing a unique rosette-like polar body showing no signal for BubR1. **(A) c)** Example of a *BicD*$^{hb\text{-}deGradFP}$ egg with only one polar body showing a weak staining for BubR1. **(A) d)** *BicD*$^{hb\text{-}deGradFP}$ egg with several meiotic products that are negative for BubR1. **(A) d')** magnified images of the indicated nuclei observed in d).
(B) a) Shows an example of the unique polar body rosette structure observed in a control egg (derived from a *BicD::GFP, BicD*^{null}), were Mad2 is present at the polar body kinetochores. **(B) b)** Shows a *BicD*$^{hb\text{-}deGradFP}$ egg where the unique rosette-like polar body present shows no signal for Mad2. **(B) c)** Example of a *BicD*$^{hb\text{-}deGradFP}$ egg with only one polar body that shows a weak staining for Mad2. **(B) d)** *BicD*$^{hb\text{-}deGradFP}$ egg where the female meiotic products have

replicated and are negative for Mad2 staining. Scale bars represent 5 μm.. Images are z-stack projections though the nuclei. Scale bars represent 5 μm.

Figure 6. Localization of D-TACC, Msps and Clc at the meiosis II tandem spindles is affected in *BicD*$^{hb\text{-}deGradFP}$ eggs. (A) 0-5 min old eggs laid by females expressing maternally a Chc::mcherry fusion protein were stained for α-tubulin (green). Chc::mCherry signal (red) was directly detected to visualize the Chc fusion protein localization. Chc is clearly present along both metaphase II tandem spindles (arrows) and at the central aster (arrowhead). Scheme of the Metaphase II tandem spindle. DNA is shown in blue. Interpolar MTs are shown in green and kinetochore microtubules in gray. Minus ends (-) and plus ends (+) of MTs are marked. The central aster is drawn as a green ring with emanating MTs with antiparallel +/- directed MTs. **(B)** Wild type embryos were stained for BicD (red) and α-tubulin (green). BicD was detected in the cytoplasm but neither excluded from nor enriched at the meiotic spindles. **(C-E)** 5 min collections of control (laid either by *BicD::GFP, BicD*^{null} homozygous mothers in C-D or wild-type mothers in E) and *BicD*$^{hb\text{-}deGradFP}$ embryos were stained for α-tubulin (red) and either D-TACC **(C)**, Msps **(D)** or Clc **(E)** (green). DNA is shown in blue. The pictures represent maximum projections of several frames. The spindle shown on top is the more superficial one in the embryo. The signal is stronger for this spindle and the signal on the spindle below is often masked by the cytoplasmic signal in the upper frames. For images in E, the images were subject to bleach and depth correction in Image J (see methods). Images were acquired in a way that the signal in the central aster is maximum but bellow saturation for all spindles. Examples of embryos in Metaphase II and Anaphase II are shown. **(C)** D-TACC is clearly enriched in the central aster (arrowhead) and along the meiotic spindles (arrows) in control embryos. In *BicD*$^{hb\text{-}deGradFP}$ embryos, the signal on the spindles is reduced compared to the signal intensity on the central aster. **(C')** The percentage of embryos showing a strong (+), a weak (+/-) or no (−) signal for TACC along the spindle (compared to the enrichment at the central aster) is shown for both genotypes. **(D)** Msps is localized to the central aster (arrowhead) and at the tandem spindles, where it is enriched at the minus end poles in control embryos (arrowheads). In *BicD*$^{hb\text{-}deGradFP}$ embryos, the signal at the spindle was reduced compared to the signal observed at the central aster. Sometimes the signal at the poles, although weak, could still be observed. **(D')** The percentage of embryos showing a strong (+) or very weak or no (−) signal for Msps along the spindle is shown for both genotypes. **(E)** Clc localization in metaphase tandem spindles. Clc is localized along the spindles and at the central aster. In embryos with reduced BicD levels, although Clc signal can still be observed along the tandem spindles, there was an unusual accumulation of Clc at the central aster. (E') The percentage of embryos showing a normal (+) or a reduced spindle

localization compared with an unusual enrichment of Clc at the central aster (−) is shown for both genotypes. (N) Number of embryos scored for each genotype was the sum of the embryos imaged from two independent immunostainings experiments. Scale bars represent 5 µm**.**

Figure 7. *Drosophila* Chc binds to D-TACC through the same domain it interacts with BicD. (A) Interaction tests in the yeast two-hybrid system. The full-length (FL) and two different fragments of Chc (aminoacids 329-542 and 329-803) were fused to the DNA binding domain (BD). Full-length D-TACC wild type (WT) and *TACC*^{S863A} were fused to the activator domain (AD). Empty vectors were used as negative controls. Full-length Chc and Chc (aa 329-803; the region that interacts with BicD**)**, interact with D-TACC. The interaction was not affected by the *D-TACC*^{S863A} mutation. **(B)** IP of total embryo extracts expressing a Myc-tagged Chc fusion protein (Myc::Chc). Antibodies used for the IPs are indicated on top. Anti-BicD antibodies (4C2 and 1B11), anti-Myc antibody and beads alone as a negative control were used. As an additional negative control, total wild-type (wt) embryo extract was used for pull down with anti-Myc antibodies. Western blots of the precipitated material were tested for the presence of BicD, Clc, D-TACC and Myc::Chc. 0.15% of the cytoplasmic extract used for each IP was loaded as input. Lower panel show a longer exposure of the Myc::Chc signal.

Figure 8. *d-tacc* is needed in the mother for pronuclear fusion and replication of parental chromosomes in the embryo. *Wild-type* embryos and embryos laid by *d-tacc*^{1} */Df 3R(110)* mothers crossed to wild-type males were subjected to DNA *in situ* hybridizations with probes detecting the X chromosome (white) and the Y chromosome (red). α-tubulin (green) and DNA (Blue) were also stained. For each genotype, examples of male embryos are shown. For wild type, an embryo in the first mitotic cycle (upper panel) and an embryo that went through several mitoses (lower panel) are shown. In both embryos, the zygotic internal nuclei contain a clear signal for the X and the Y chromosomes. The remaining polar body (seen only in the upper embryo) contains a clear signal only for the X chromosome. Note that a very weak, but unspecific, signal for the Y chromosome (probably due to weak cross reactivity to the 2nd or 4th chromosome) is observed in some of the female meiotic polar bodies in wild type and *d-tacc*^{1} mutant embryos. In *d-tacc*^{1}**,** polar bodies are marked by the presence of the X chromosome, however zygotic internal nuclei marked only by the presence of the Y chromosome are observed, indicating a problem in pronuclear fusion. Images are z-stack projections though the nuclei.

Figure 9. Knockdown of *BicD* in *Drosophila* tissue culture cells affects mitosis. BicD and Chc genetically interact in cells and embryos.

S2 *Drosophila* cells were incubated with dsRNA against *BicD, Chc, Clc* or a combination of them. Cells transfected with dsRNA against *GFP* were used as control. Double amount of dsRNA against *GFP* was used (*2xGFP*) for controls of double knockdown cells. Knockdowns were done in triplicates (1 to 3). **(A,D)** Western Blot showing the efficient knock down of the proteins after 3 days of dsRNA treatment detected with anti-BicD or Clc antibodies. α-tubulin levels were used as loading control. Anti-Clc was used to detect degradation of Chc and Clc since RNAi against one Clathrin subunit reduces the levels of both subunits. **(B, D)** The percentage of abnormal cells, either showing more than two or fragmented centrosomes (Cent.) (black bars) or multipolar spindles (gray bars) is depicted in the graphs for each treatment and plotted as the difference with the corresponding dsRNA against the corresponding GFP control. *Drosophila* tissue culture cells are known to display certain level of such defects due to polyploidy. However, cells treated with *dsRNA* against *BicD, Chc* and *Clc* showed an enhancement of these phenotypes. Double knock down of *BicD* and either *Chc* or *Clc* reduced the number of abnormal mitoses. 120 to 200 cells were counted for each individual treatment. Error bars represent SE of the difference in means between the treatments. **(C)** Examples of the spindle phenotypes observed. Cells were stained for α-tubulin (red), Cnn (green) and DNA (blue). Normal cells are expected to have bipolar spindles and two centrosomes (Cent.). Scale bars are 5 μm. **(F)** Percentage of embryos that hatched into larvae. The depicted genotypes are the ones of the mothers (crossed to *wild-type* males) that laid the eggs. **(G)** Embryos laid by the same mothers as in A were collected and aged 2 to 5 h. After fixing, they were stained with Hoechst and with anti α-tubulin to follow their development. The percentage of developed embryos was counted for each maternal genotype.

Figure 10. *C. elegans chc-1* and *tac-1* are required for meiosis and pronuclear fusion.

Images from fluorescent microscopy time-lapse sequences **(A-E, G)** or single confocal pictures **(F, H)** of **(A)** control *(RNAi)*, **(B-C)**, *tac-1 (RNAi)* and **(D, F-G)** *chc-1 (RNAi)* and **(E)** *bicd-1 (RNAi)* embryos expressing *H2B::mCherry* and *α-tubulin::GFP*. Pictures are oriented with anterior (A) to the left and posterior (P) to the right. Female and male pronuclei are indicated in the first time-lapse micrograph. Time lapse pictures indicate the elapsed time (in minutes and seconds) from the start of the movie at 00:00 with the female pronucleus still at the anterior. **(A)** Shows a control embryo that developed normally. **(B)** Shows a *tac-1 RNAi* embryo where polar body extrusion is delayed (arrowhead). The female pronucleus migrated to the posterior towards the male pronucleus. Meanwhile, the male pronucleus made a

spindle on its own. Although both pronuclei met at the posterior and formed a common spindle, no fusion of pronuclear DNA is observed. **(C)** In this *tac-1 RNAi* embryo, the female pronucleus did not migrate to the posterior and pronuclear fusion did not take place. The male pronucleus formed its own spindle. **(D)** Shows a *chc-1 (RNAi)* embryo where the female pronucleus migrated slowly to meet the male pronucleus at the posterior but no pronuclear fusion was observed. **(E)** Shows a *bicd-1 (RNAi)* where the female pronucleus migrated to meet the male pronucleus at the posterior but no pronuclear fusion was observed. **(F)** This *chc-1 (RNAi)* embryo arrested in metaphase of meiosis. **(G)** Shows a 2 cell stage *chc-1 (RNAi)* embryo, with premature capture of a polar body (PB). The PB DNA fused with the AB blastomere DNA. **(H)** Shows an example of a dying *chc-1 (RNAi)* embryo with vacuoles. Scale bars are 10 μm.

Supplementary Figure S1. In syncytial *Drosophila* embryos Chc and Clc localize to mitotic spindles and centrosomes throughout cell cycle. **(A)** Embryos laid by $BicD^{mom}$ females were fixed and subjected to immunostaining to detect α-tubulin (red), Cnn (green) and DNA (blue). Wild-type embryos were used as control. $BicD^{mom}$ embryos arrested in early embryogenesis showing few spindles and rosette structures. Abnormal spindles with detached and multiple centrosomes and centrosomes not associated to any DNA were observed. Scale bars are 20 μm. **(B)** Localization of a Myc-tagged Chc fusion protein (green) in embryos laid by *Nanos-Gal4 > pUASP-Myc::Chc* females. Chc is enriched apically where it further accumulates in a punctate pattern above each blastoderm nucleus (arrow). Scale bars are 30 μm. **(C)** Embryos laid by mothers having a lethal allele of *Chc* (Chc^{1}) but rescued with two copies of a Flag-tagged Chc expressed from the 4C-CHC construct (Kasprowicz et al., 2008) were stained to detect Chc and the pericentrosomal marker Cnn using anti-Flag antibodies (Red) and anti-Cnn antibodies (green), respectively. DNA is shown in blue. Both proteins co-localized at the centrosomes. A magnified region of an embryo in prophase is shown. **(D)** Embryos from mothers expressing a Chc::eGFP fusion protein (Green) (Li et al., 2010) and histone-RFP (red; to visualize the chromosomes) were subject to live imaging. Chc::eGFP localized to the centrosomes and spindles throughout the cell cycle. **(E)** Embryos from mothers expressing a Clathrin light chain (Clc) fused to GFP (Clc::GFP) under the Maternal-Tubulin promoter were devitelinized by hand to preserve the Clc::GFP signal and subjected to immunostaining to detect α- tubulin and Cnn. A magnified picture of a region of an embryo in metaphase and another in prophase are shown. Left panels show an overlay of the signals for α-tubulin (red), Cnn (green) and DNA (blue). Middle panels show the signal for DNA (blue) and Clc::GFP (green). Right panels show the signal for Clc::GFP in gray. Like Chc,

Clc is localized to the mitotic spindles and centrosomes throughout the cell cycle. The side view reveals an apical enrichment as well. Scale bars represent 10 μm in C-E.

Supplementary Figure S2. Although the deGradFP protein is detected in ovaries of *BicD*$^{hb\text{-}deGradFP}$ females, *BicD*$^{hb\text{-}deGradFP}$ stage 14 oocytes show apparently normal meiosis I spindles. (A) Ovaries from control (homozygous *BicD::GFP, BicD*^{null}) or *BicD*$^{hb\text{-}deGradFP}$ females were dissected in Robbs medium to prevent oocyte activation. They were then subjected to Western blotting using anti-Lamma IgG antibodies to detect the deGradFP fusion protein. α- tubulin was used as loading control. **(B)** Stage 14 oocytes from control (homozygous *BicD::GFP, BicD*^{null}) or *BicD*$^{hb\text{-}deGradFP}$ females were prepared and stained to detect α-tubulin (red) and DNA (blue). Metaphase I oocyte spindles were imaged. **(C)** Spindles were classified as normal, when they showed a normal bipolar appearance or as abnormal when multipolar spindles were observed. Images are confocal z-stack projections. Scale bars are 2 μm.

Supplementary Figure S3. Arrested fertilized *BicD*$^{hb\text{-}deGradFP}$ eggs show abnormal spindles with centrosomes whereas non-fertilized *BicD*$^{hb\text{-}deGradFP}$ eggs have acentrosomal spindles. (A-B) Virgin *BicD*$^{hb\text{-}deGradFP}$ females were crossed to males that expressed a fusion protein between Don Juan (Dj) and mCherry (Dj::mCherry) under the control of the endogenous *Dj* promoter. Dj associates with sperm tails, and the fertilizing sperm tail ends up in the cytoplasm of the *Drosophila* egg (Santel et al., 1997). Embryos laid by these females were collected and stained to detect α-tubulin too. mCherry fluorescence was preserved with MetOH fixation. **(A)** Dj:mCherry can be detected on the sperm tail only in young embryos (with few zygotic nuclei) . **(B)** After Dj::cherry is shed from the sperm tail during the first mitotic divisions, the presence of the sperm tail could still be followed for some time during the late syncytial divisions with α-tubulin staining that detects the sperm tail also in older embryos. Images are confocal z-stack projections. Scale bars represent 25 μm.

Supplementary Figure S4. Unfertilized *BicD*$^{hb\text{-}deGradFP}$ eggs produce abnormal meiotic products that undergo extra rounds of replication.

Control (homozygous *BicD::GFP, BicD*^{null}) and *BicD*$^{hb\text{-}deGradFP}$ virgin females were crossed to XO males to collect unfertilized eggs. Eggs were subjected to DNA *in situ* hybridization with a probe that detects the presence of the 2nd chromosome (white), α-tubulin (green) and DNA (Blue). **(A)** Eggs in control samples show normal completion of meiosis. Magnified pictures of the meiotic products observed in two different eggs are shown (a, a'). In *a,* the four meiotic products have fused into a single polar body with a rosette shape. In the egg depicted in *a'* the

meiotic products have fused into two rosette-like structures. The polar bodies in each egg contain in total four dots of signal for the 2nd chromosome, corresponding to the four meiotic products that are produced after normal completion of meiosis II. **(B)** (b) Example of a *BicD*$^{hb\text{-}deGradFP}$ egg showing the presence of a single big nucleus without the typical rosette-like structure. The chromatin appears de-condensed with many signals for the 2nd chromosome. (*b'*) A *BicD*$^{hb\text{-}deGradFP}$ egg that has three meiotic products without the typical rosette-like appearance. In all nuclei, the second chromosome probe generates many dots. (*b"*) Egg with many meiotic products marked with numerous 2nd chromosome signals. Images are confocal z-stack projections. Scale bars represent 10 μm.

Supplementary Figure S5. *Drosophila* Chc uses the same region to interact with both BicD and D-TACC in the yeast two-hybrid system **(A)**. Interaction test of full-length and BicD C-terminal Domain (CTD) fused to the DNA activation domain (AD) with Chc full-length (FL) and a Chc fragment comprising aminoacids 329 to 542 fused to the DNA binding domain (BD). Full-length Egl was used as positive control for the interaction. BicD FL and BicD CTD interact with full length Chc but not with the short fragment. **(B)** Interaction test of the elongated Chc fragment (aminoacids 329-807) fused to the AD with BicD FL and BicD CTD in the BD. The extended fragment can interact with the BicD CTD. **(C)** Interaction test between Chc FL with D-TACC wild type (WT), *D-TACC*^{S863A}, and *D-TACC*^{S863D}. Chc interacts with all D-TACC variants, but the interaction is stronger with *D-TACC*^{S863D}. **(D)** Interaction test of BicD CTD in the BD with the same versions of D-TACC used in C. No interaction between BicD and D-TACC was observed. Egl was used as positive control to test the interaction with BicD. Empty vectors were used as negative controls.

Supplementary Figure S6. Knockdown of one Clathrin subunit reduces the levels of both subunits in *Drosophila* cells in culture. *Drosophila* S2 cells from the experiment shown in Fig. 10 were subjected to western blot **(A)** and Immunofluorescence **(B)** to confirm the knockdown of Chc and Clc, respectively. Briefly, the cells were incubated with dsRNA against *BicD, Chc* or *Clc*. Cells transfected with dsRNA against GFP were used as controls. **(A)** Western blot showing the efficient knock down of Chc and BicD after 3 days of dsRNA treatment. α-tubulin levels were used as loading controls. Treatment of the cells with Clc RNAi also led to a knockdown of Chc. (Knockdown of Clc upon Chc RNAi treatment is shown in Fig. 10) **(B)** After knockdown with the indicated RNAi, cells were subjected to immunofluorescence to detect Clc (green), α-tubulin (red) and DNA (blue). The signal for Clc was reduced upon Chc and Clc RNAi knockdown**.**

Supplementary Figure 7. The few *BicD*$^{hb\text{-}deGradFP}$ embryos that continue through the syncytial mitotic divisions are enriched for embryos in metaphase. Females of the depicted genotypes were crossed to wild type males. 30-60 min old embryos were collected, stained with anti α-tubulin antibody to detect the spindles (red), anti-Cnn to mark the centrosomes (green) and Hoechst to visualize the DNA (blue). The few embryo that went through the 2nd mitotic division were counted and scored as being in: prometaphase/metaphase (PM/M), anaphase (A), telophase (T) and interphase or prophase (I/P). Two independent collections were classified and counted. The graph shows the average and the SD. The n values depicted in the picture are total numbers of embryos scored.

Fig. 1

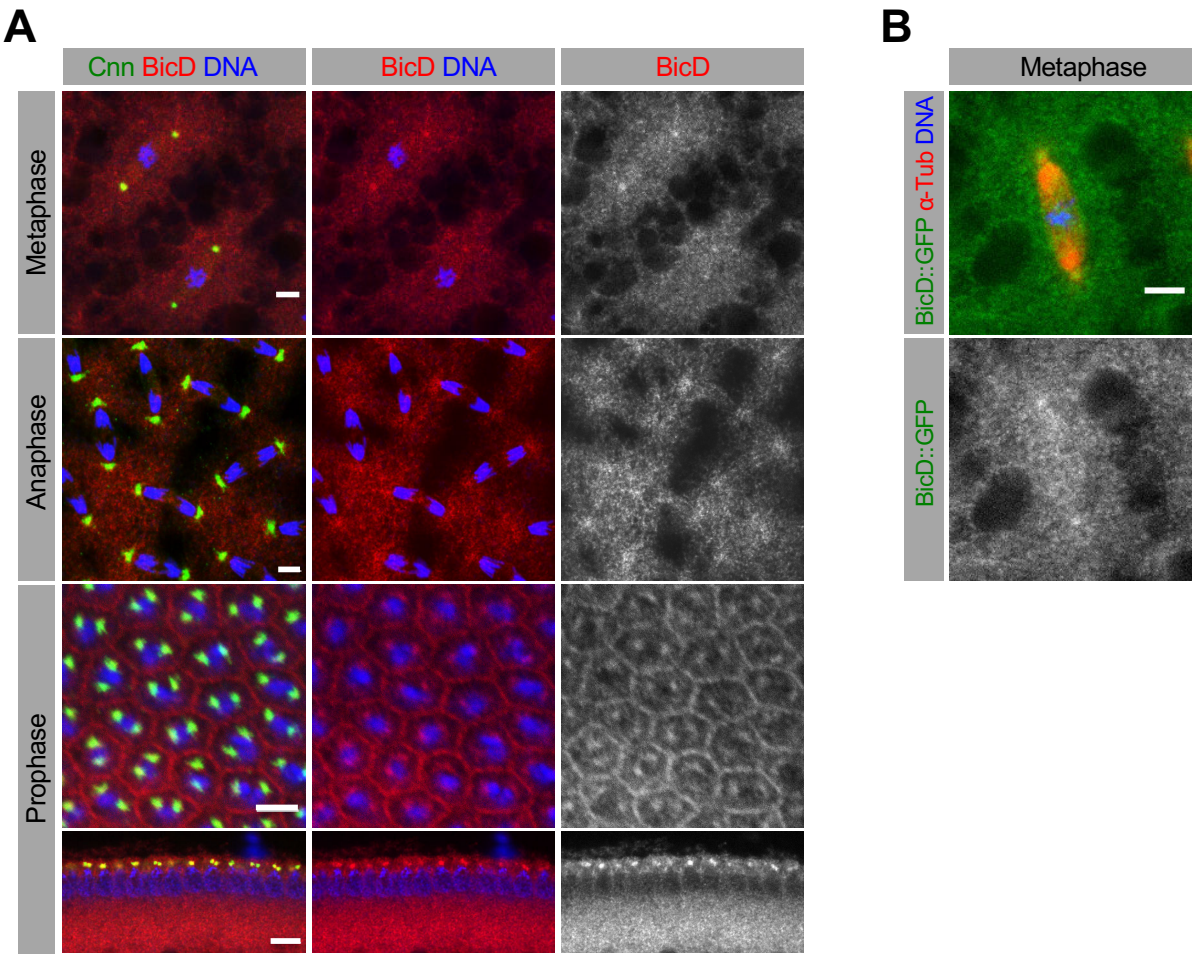

Mat-tub-Gal4 >>UAS-Chc::V5

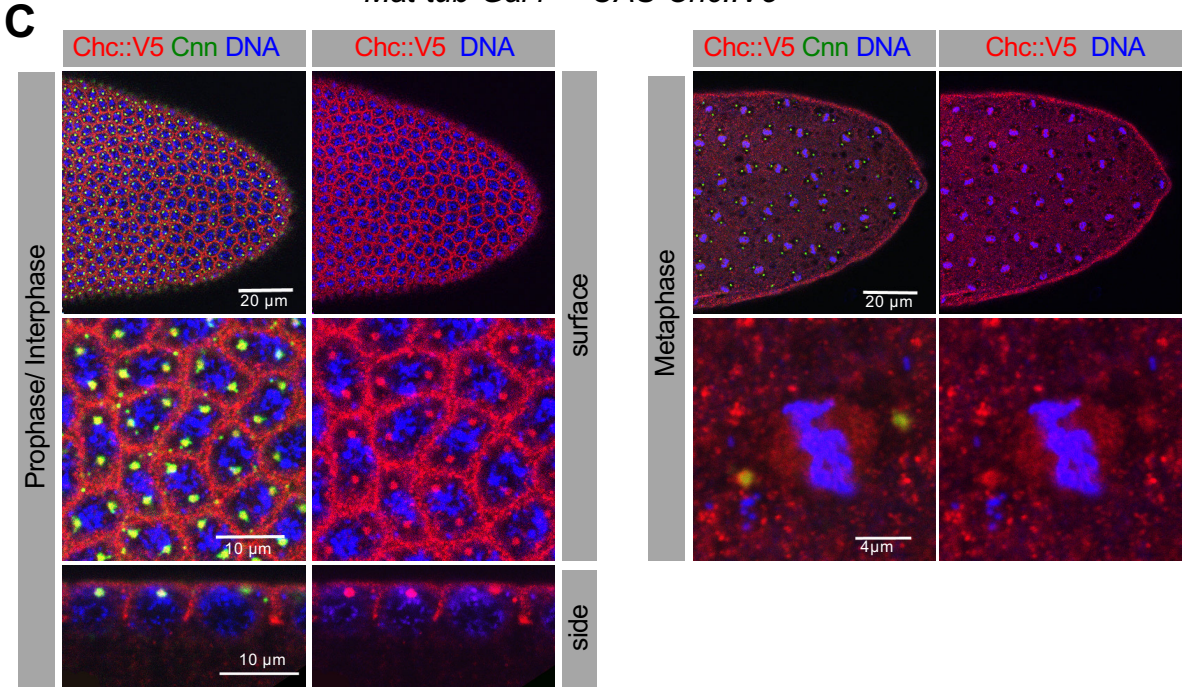

Nos-Gal4 >>UAS-Chc::mCherry

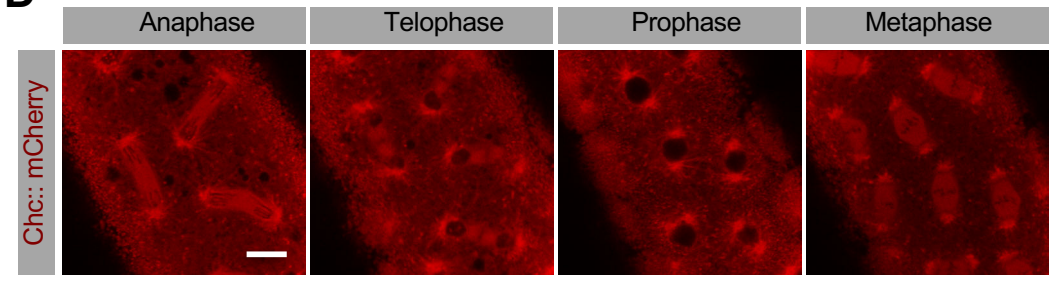

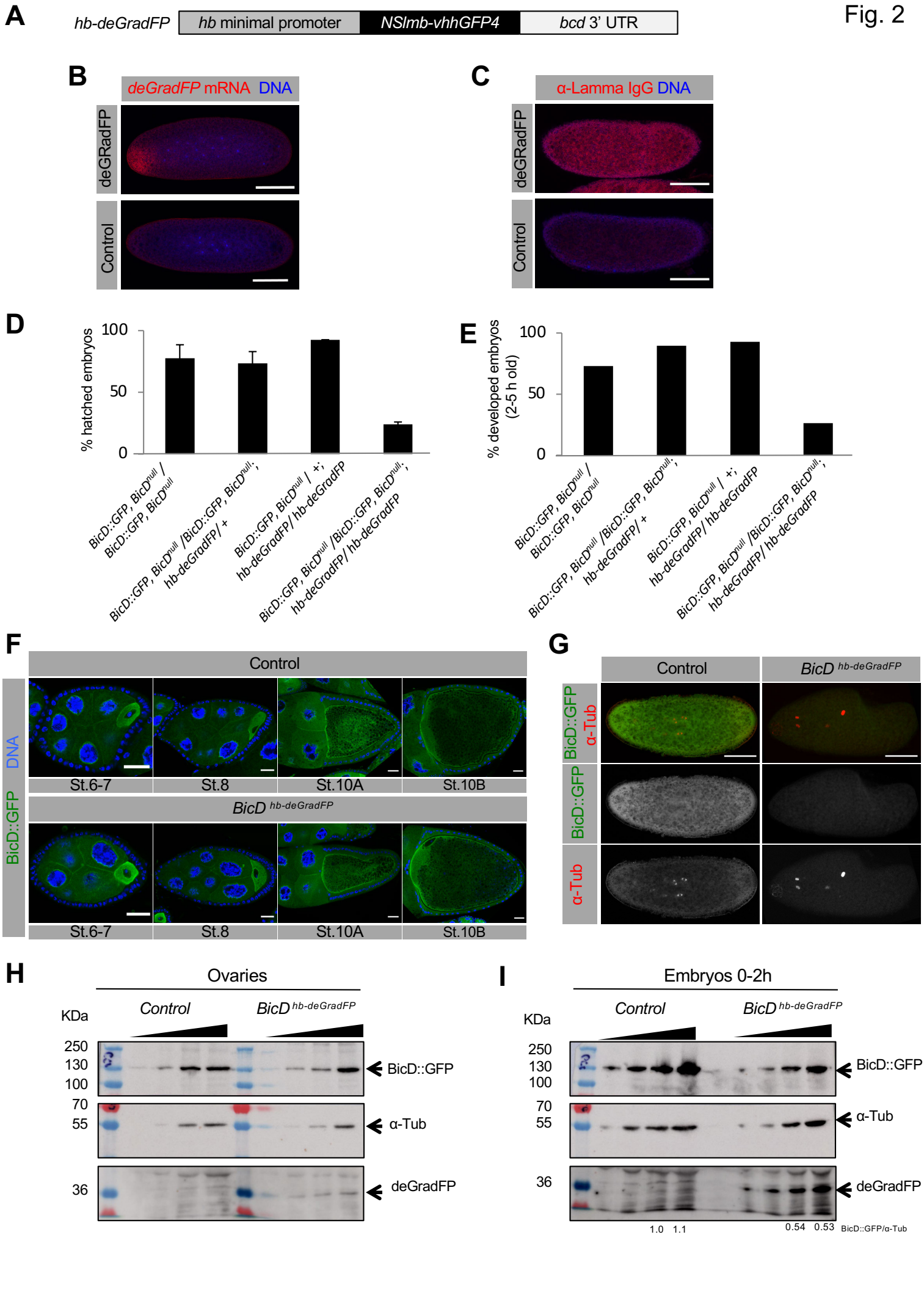

Fig. 3

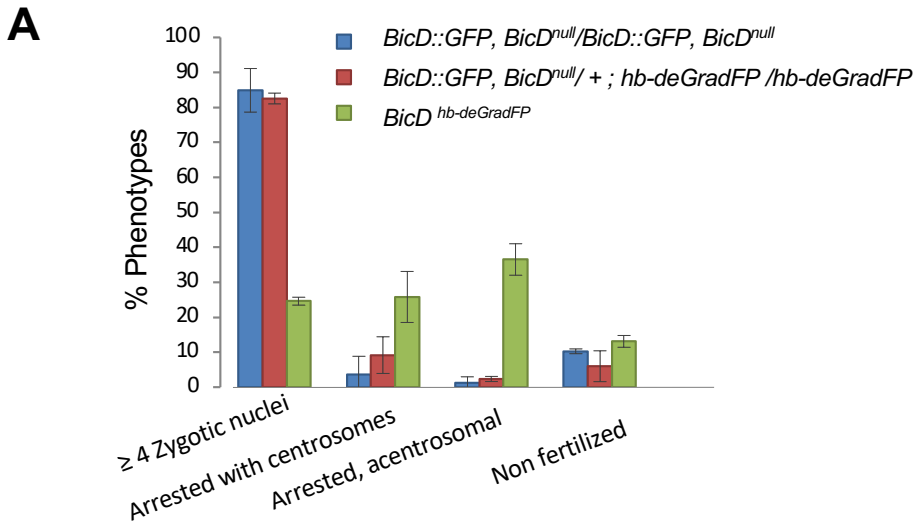

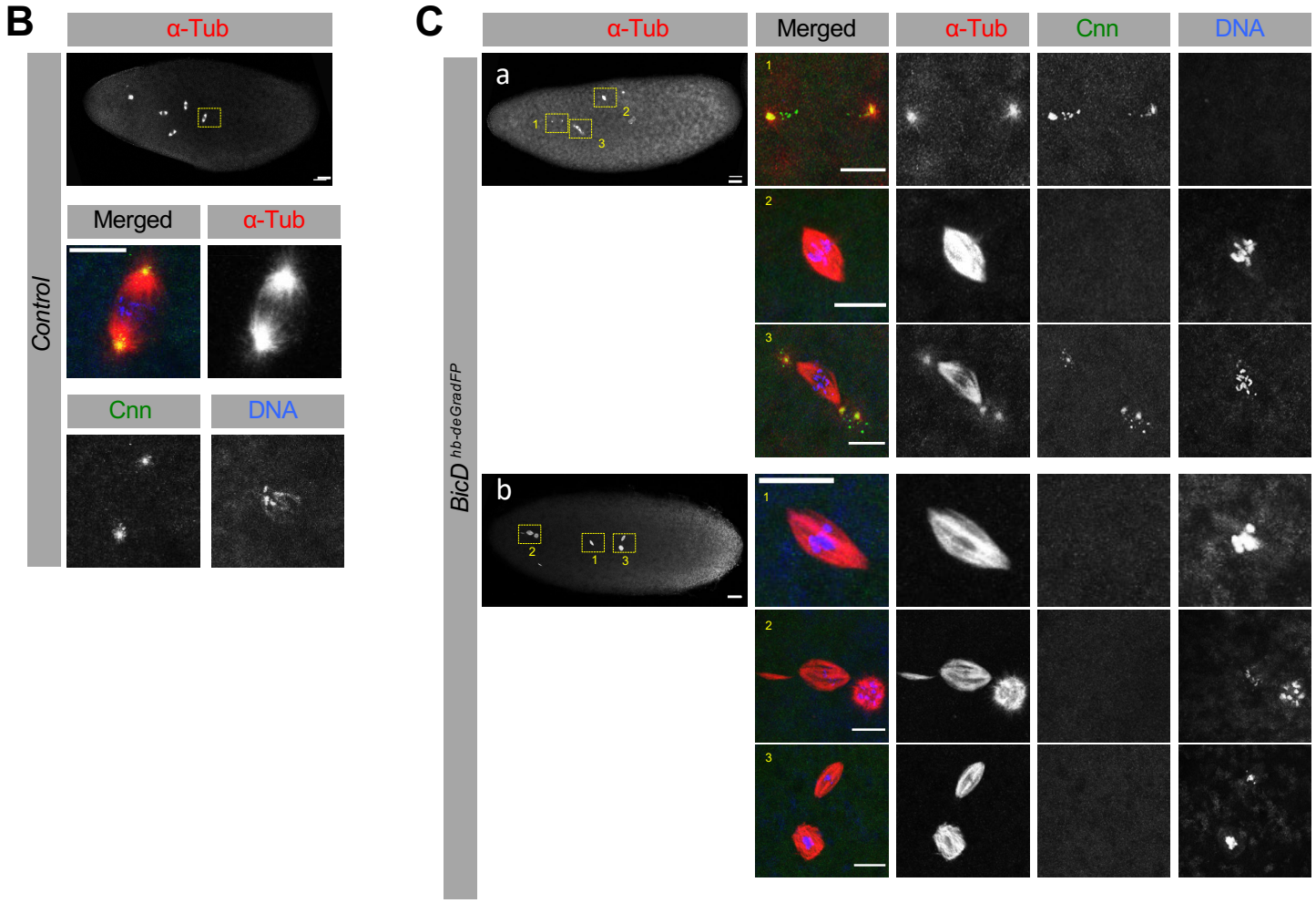

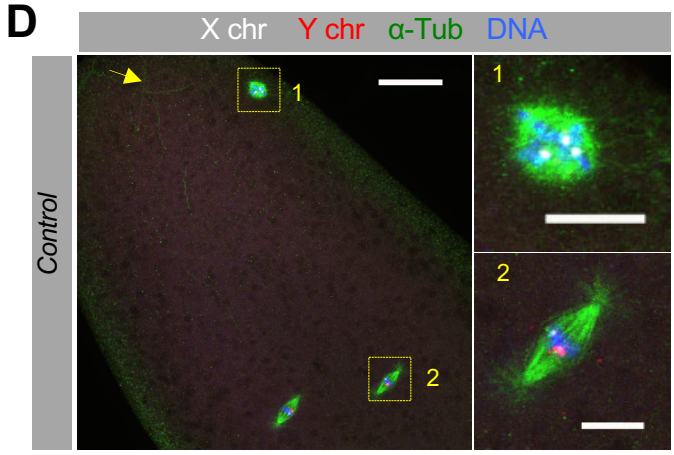

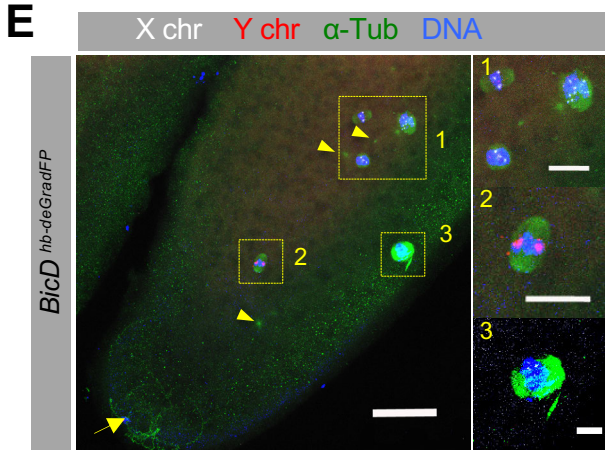

Fig. 4

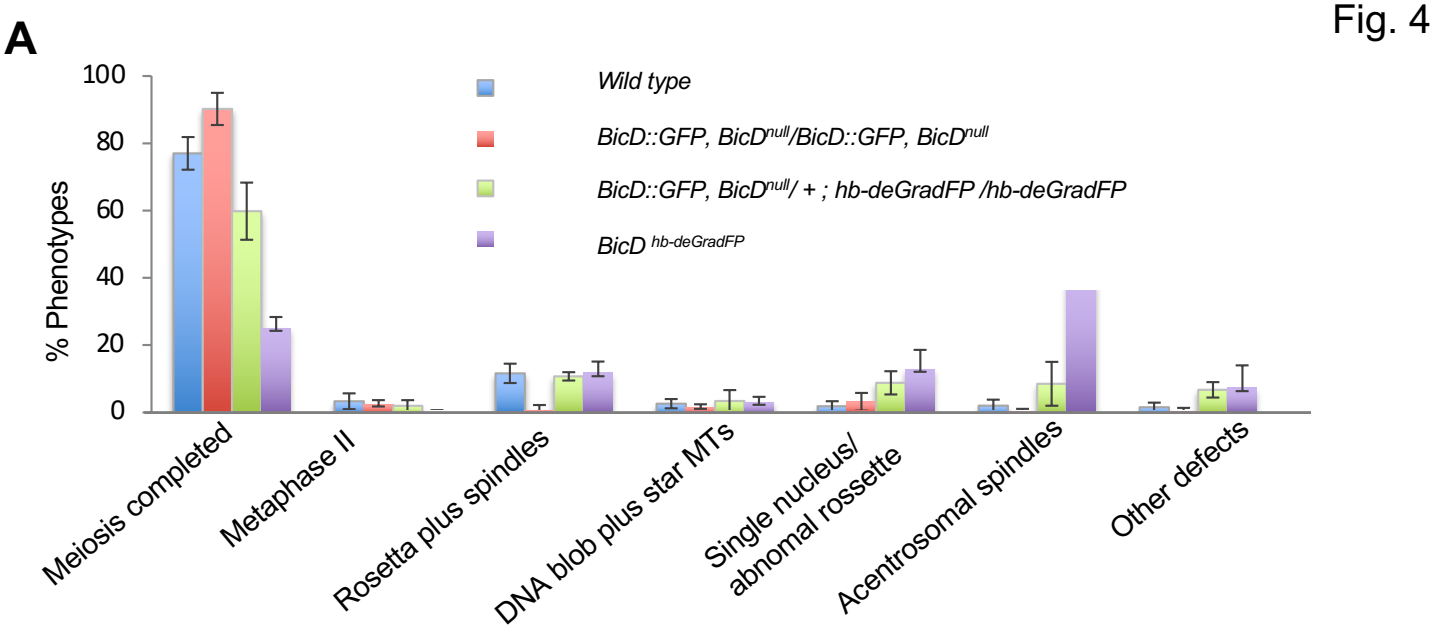

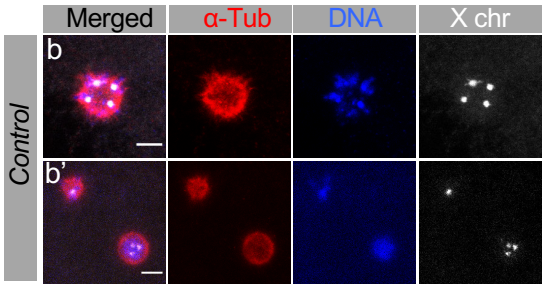

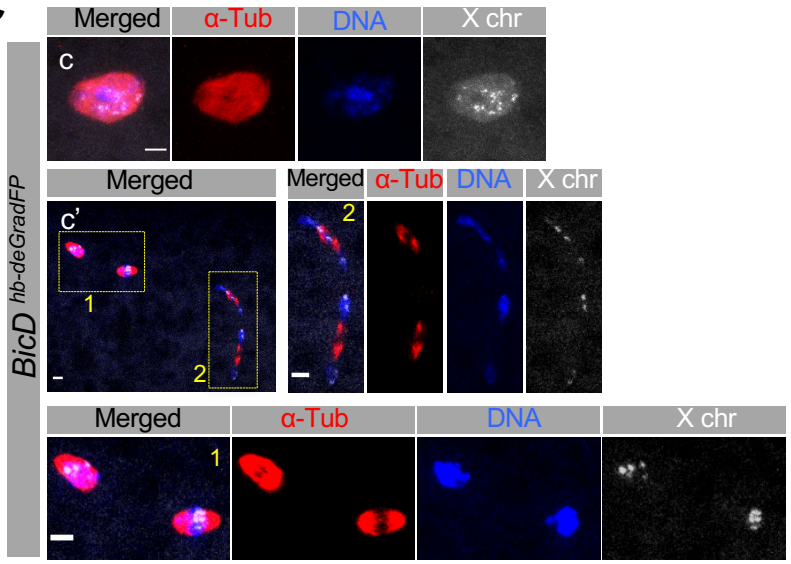

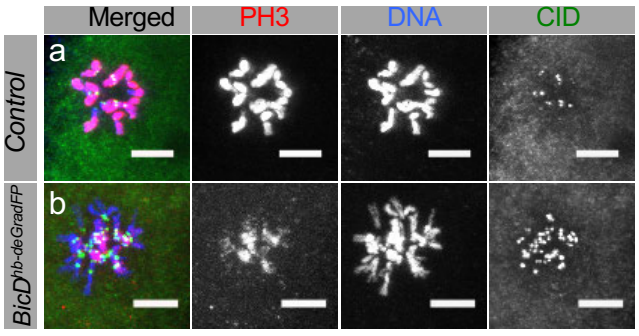

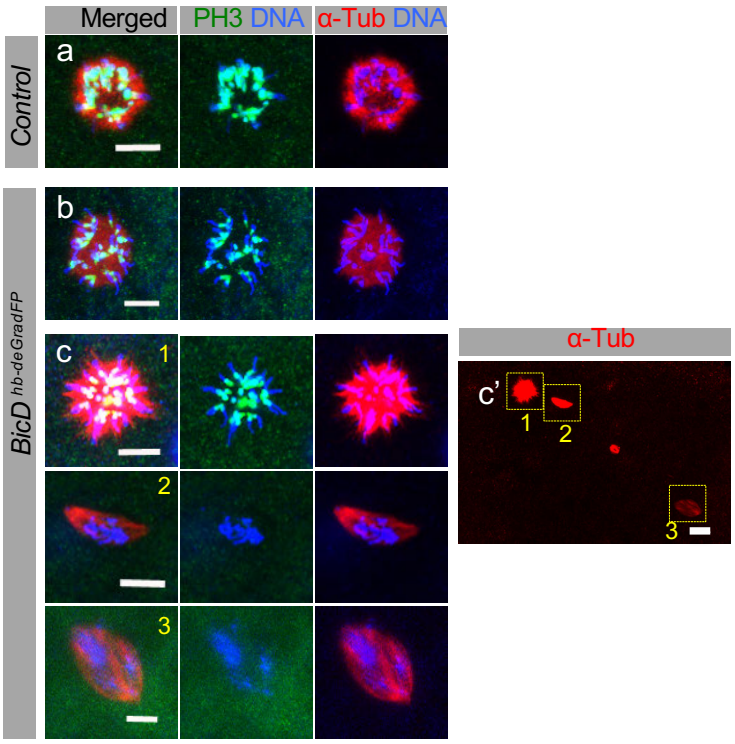

Fig. 5

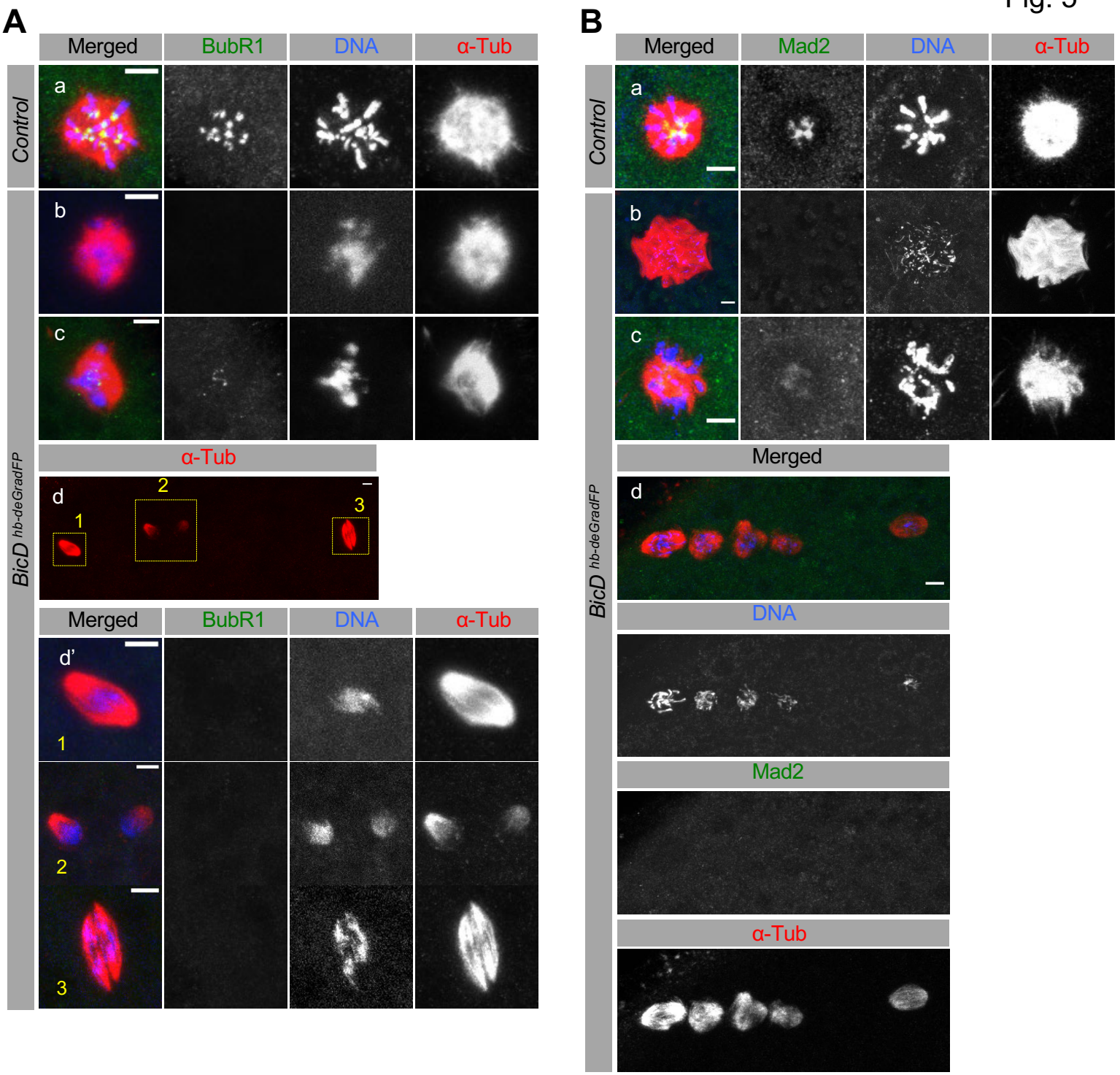

Fig. 6

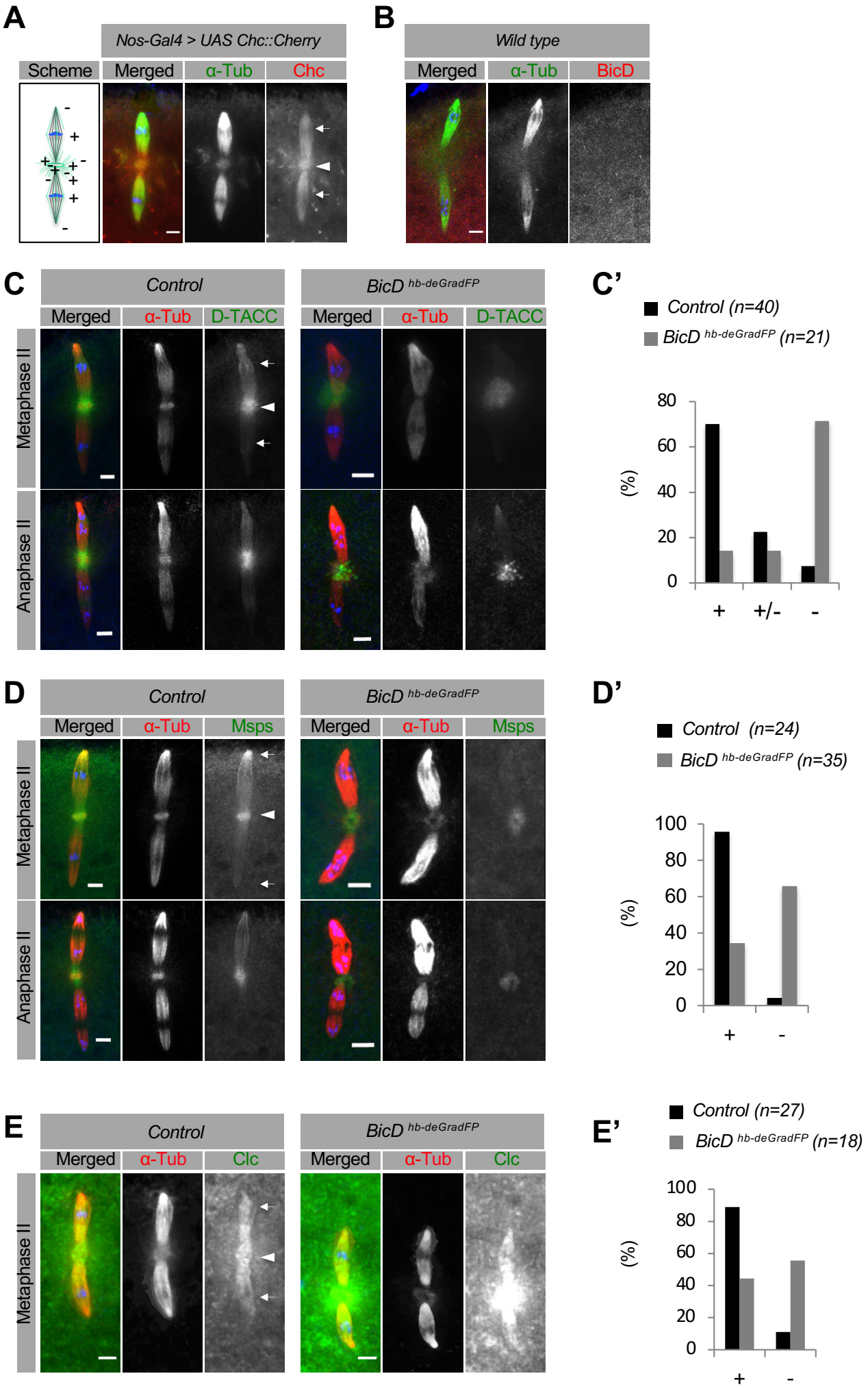

Fig. 7

A

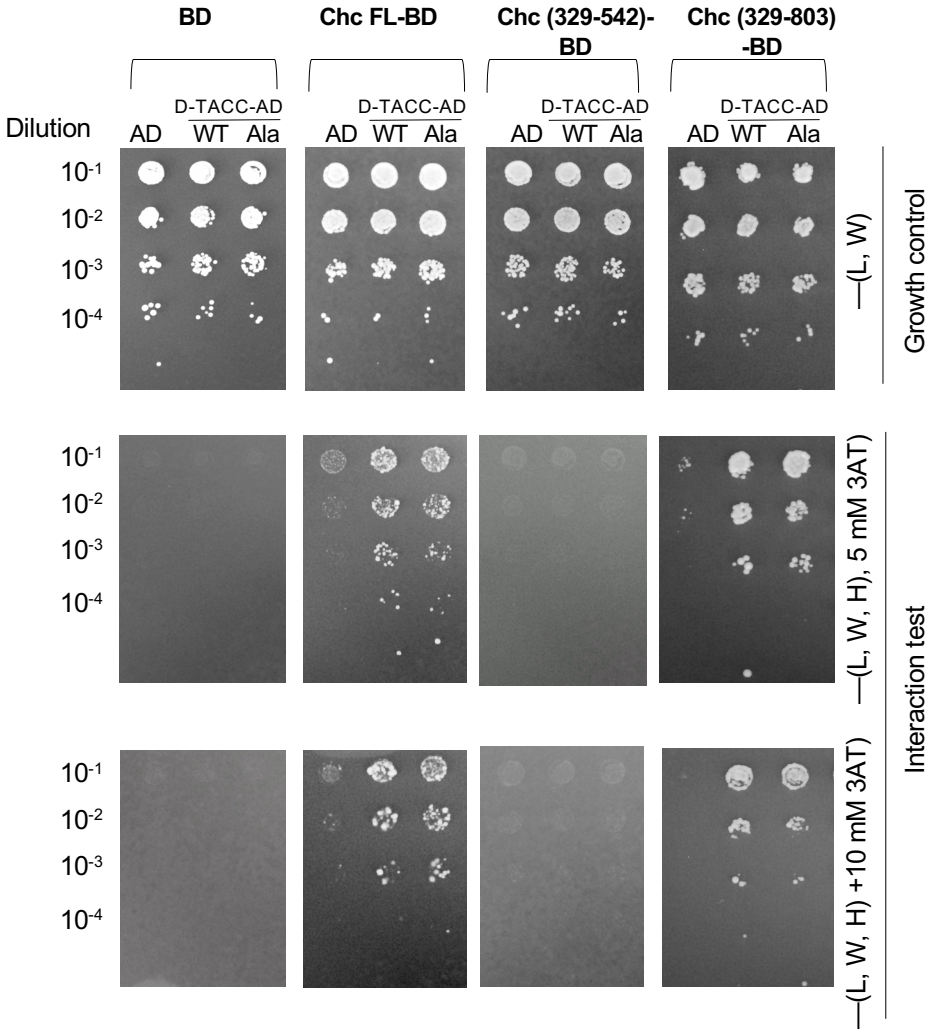

B

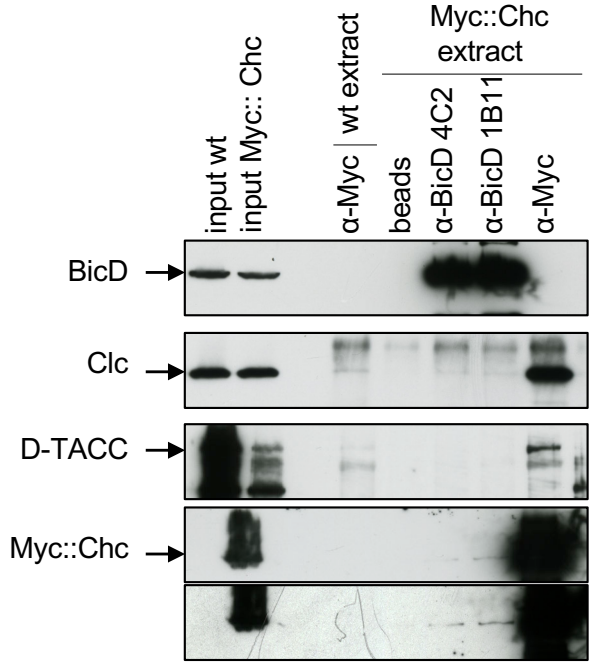

Fig. 8

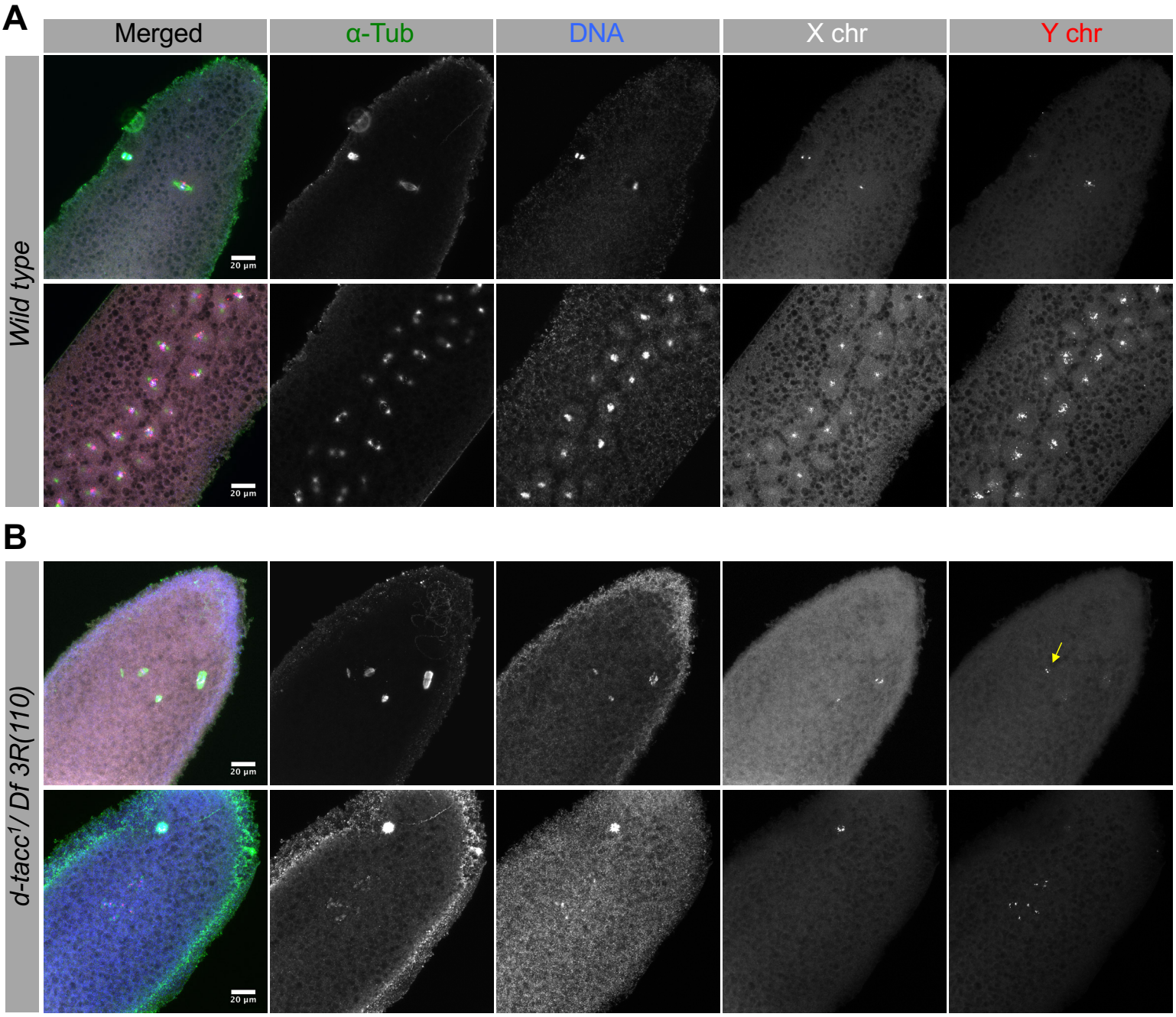

Fig. 9

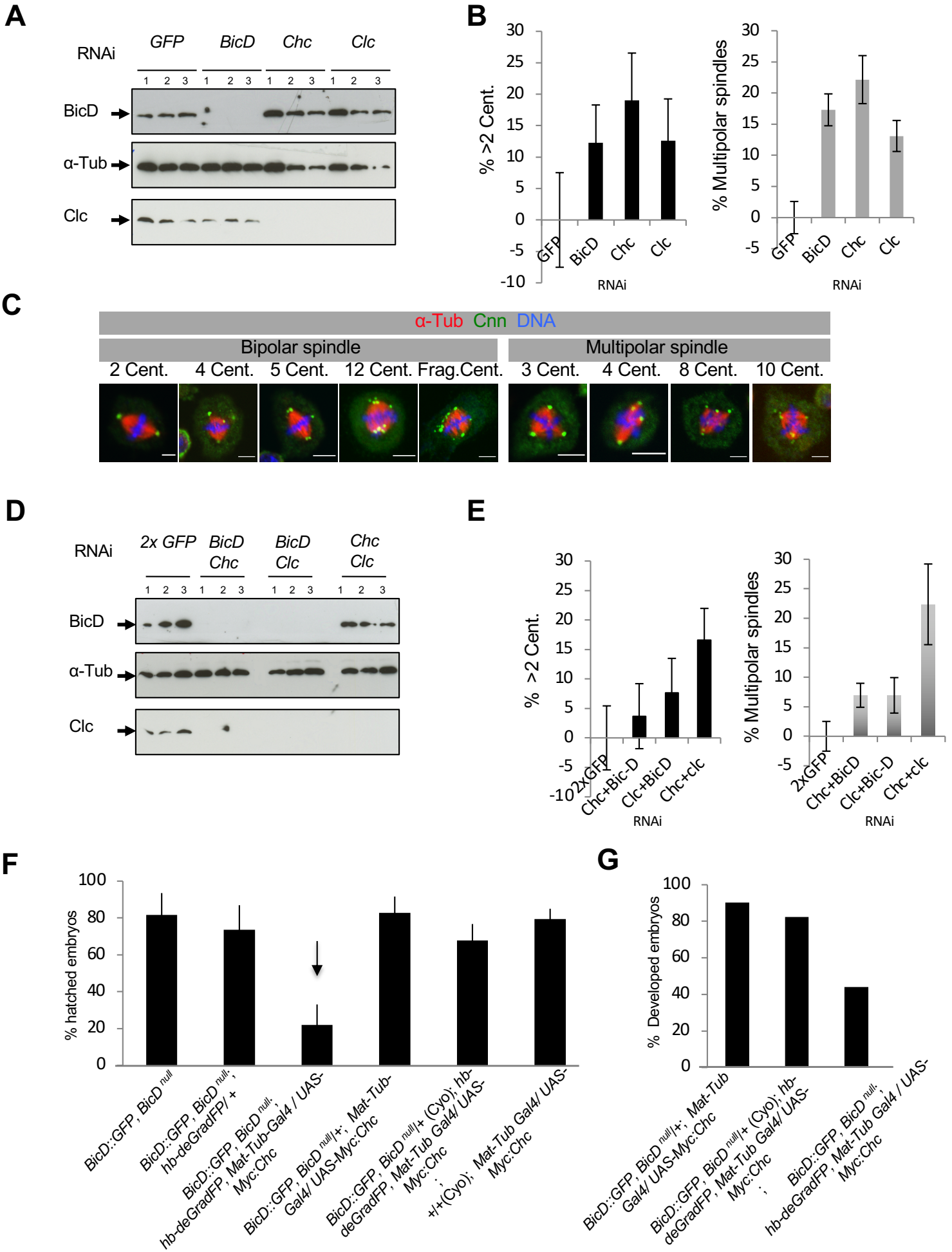

Fig. 10

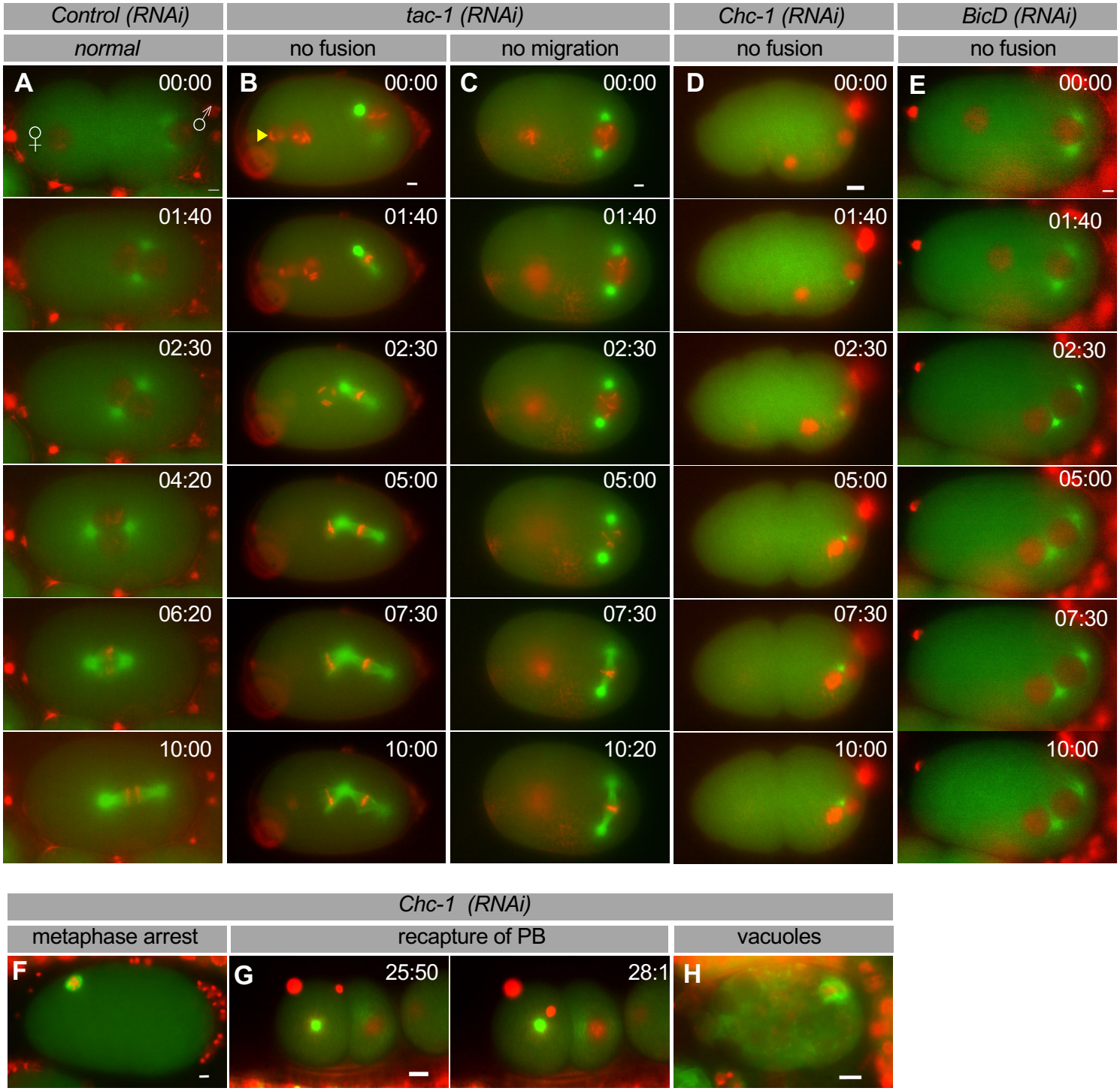

Supplementary Fig. S1

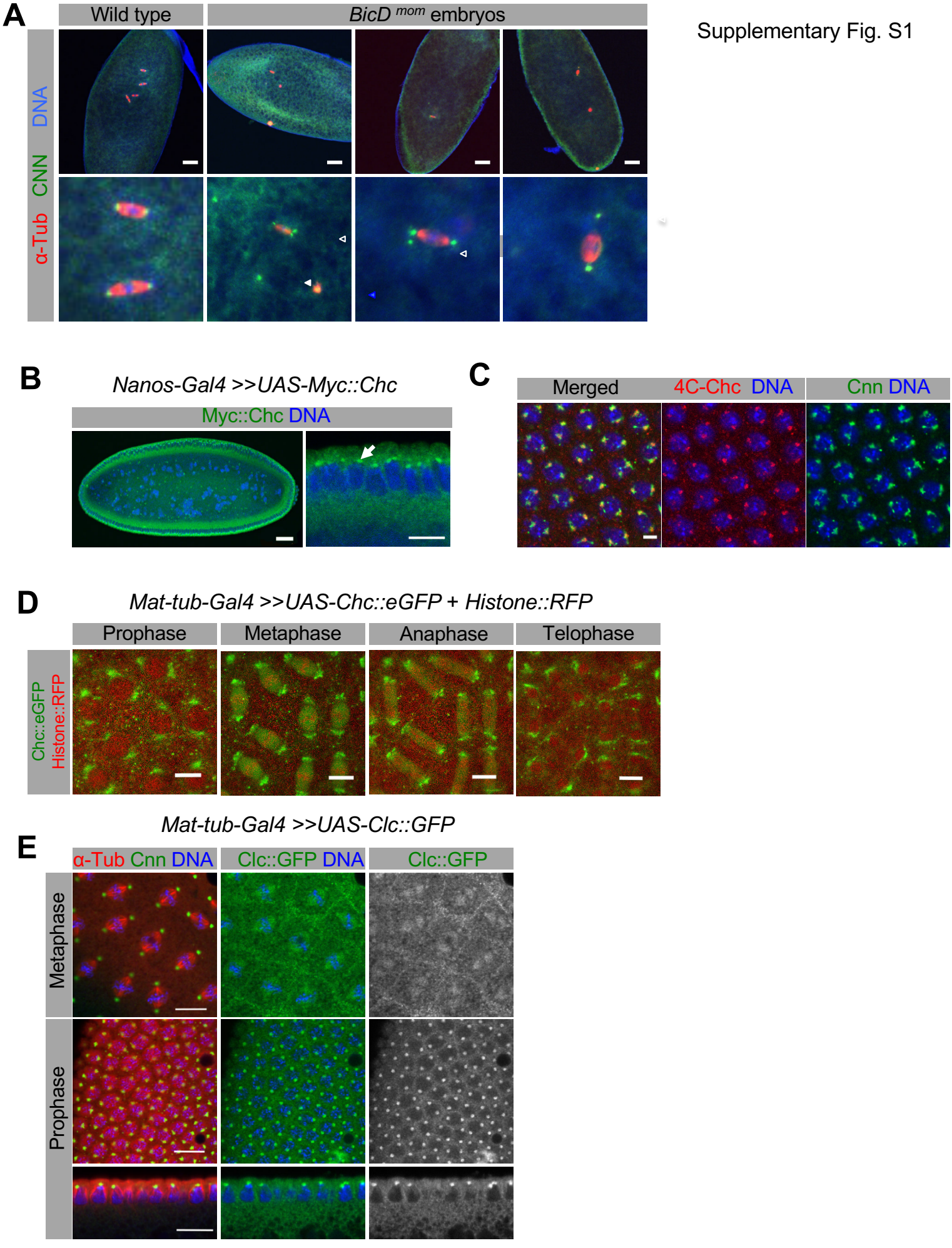

Supplementary Fig. S2

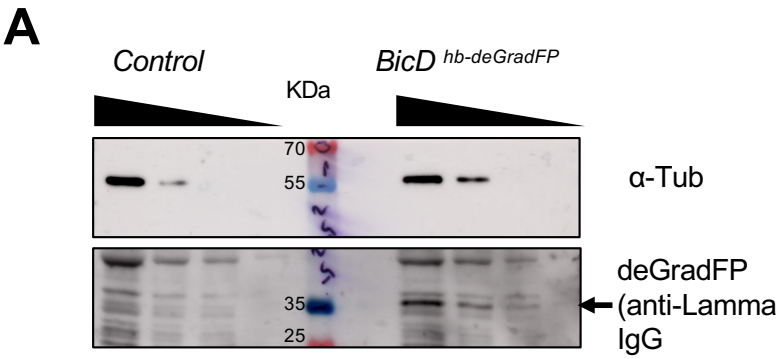

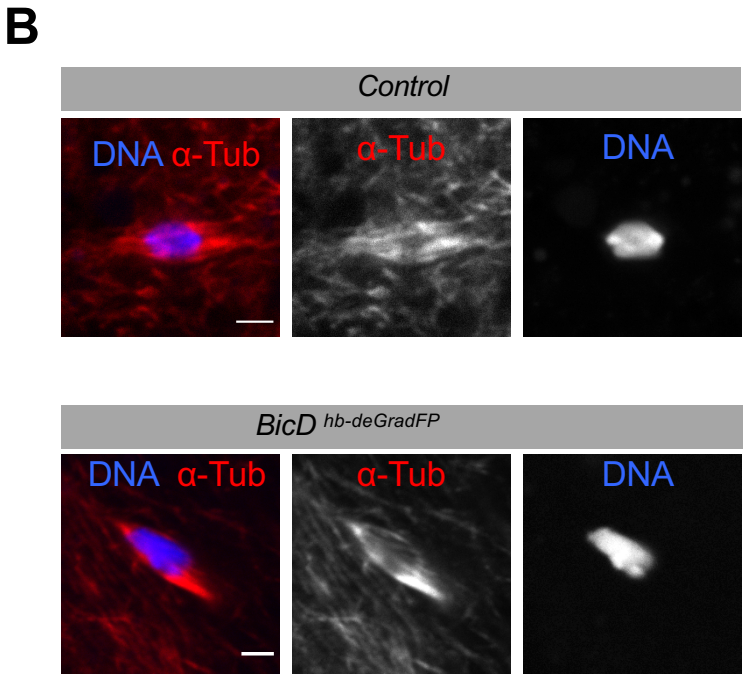

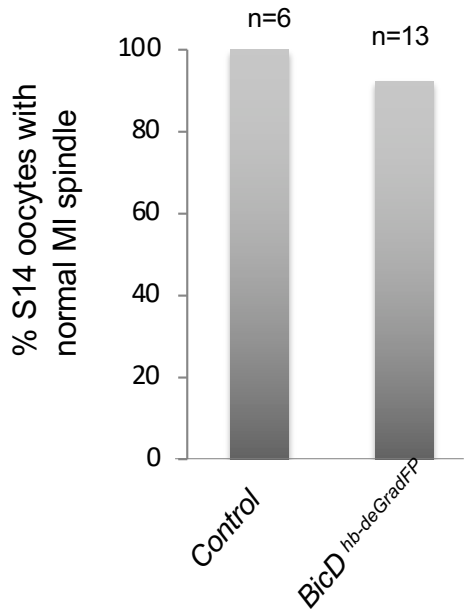

Supplementary Fig. S3

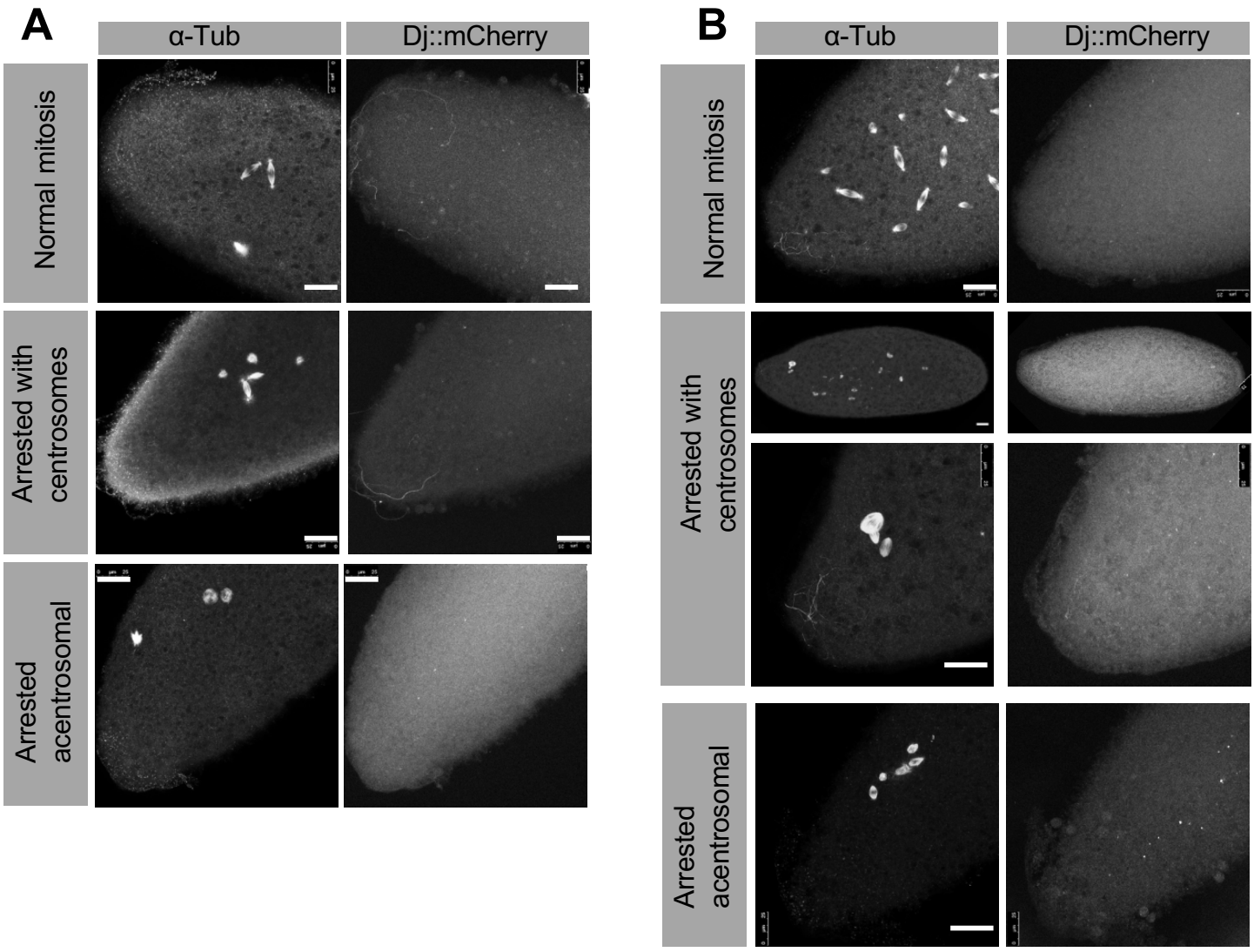

Supplementary Fig. S4

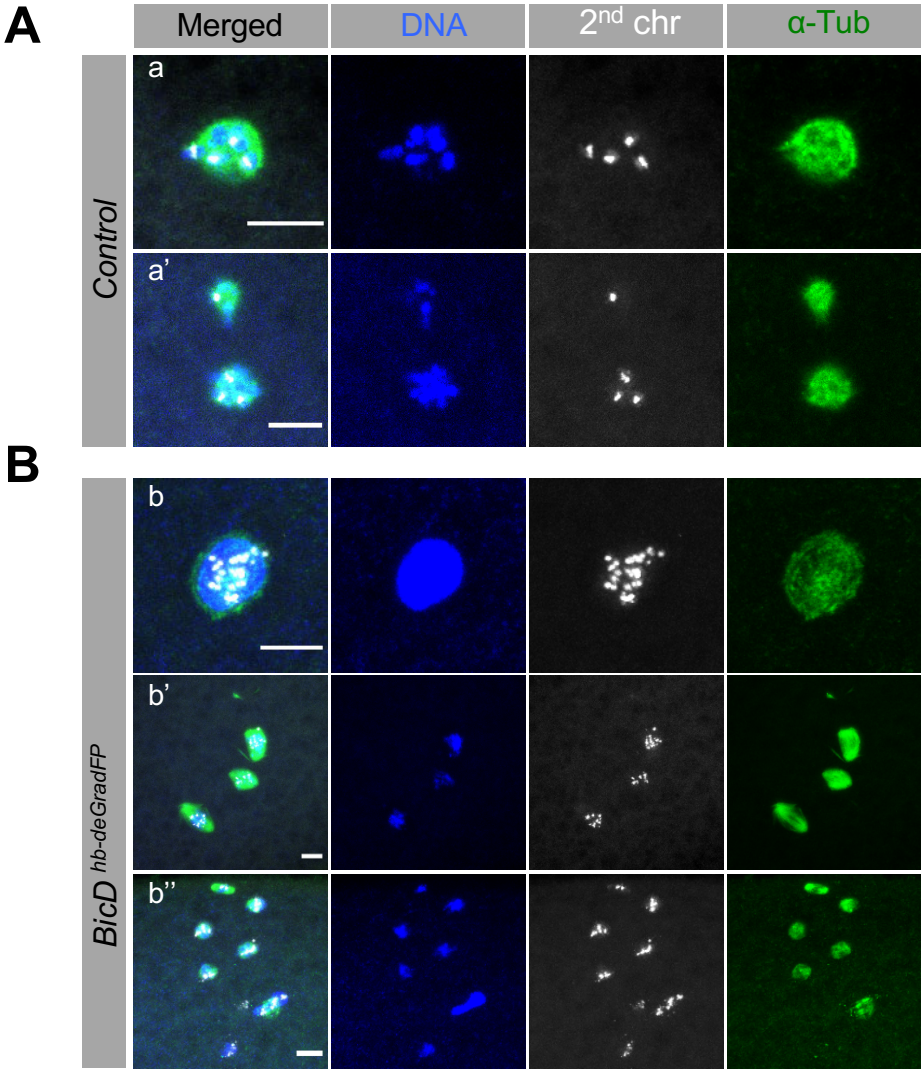

Supplementary Fig. S5

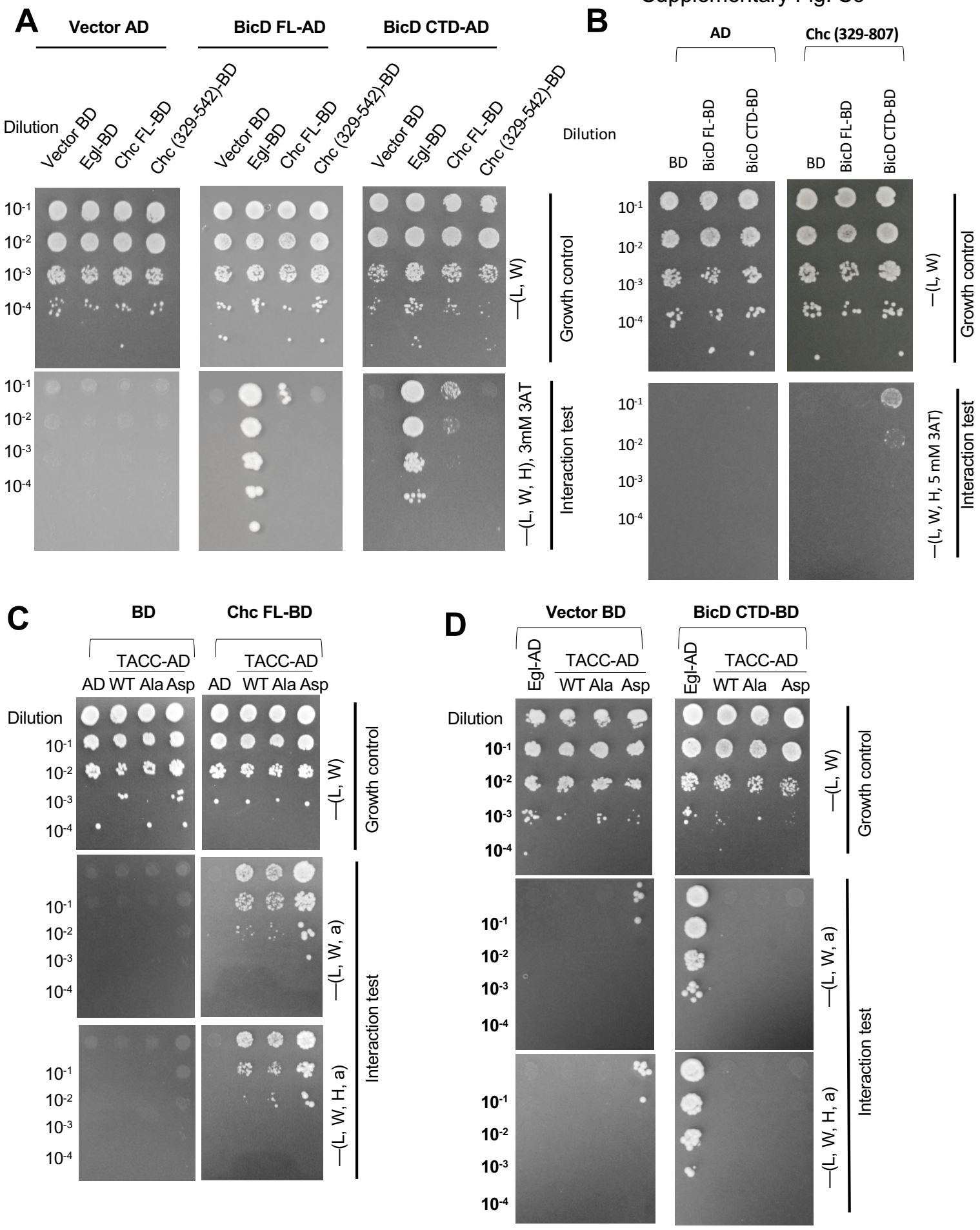

Supplementary Fig. S6

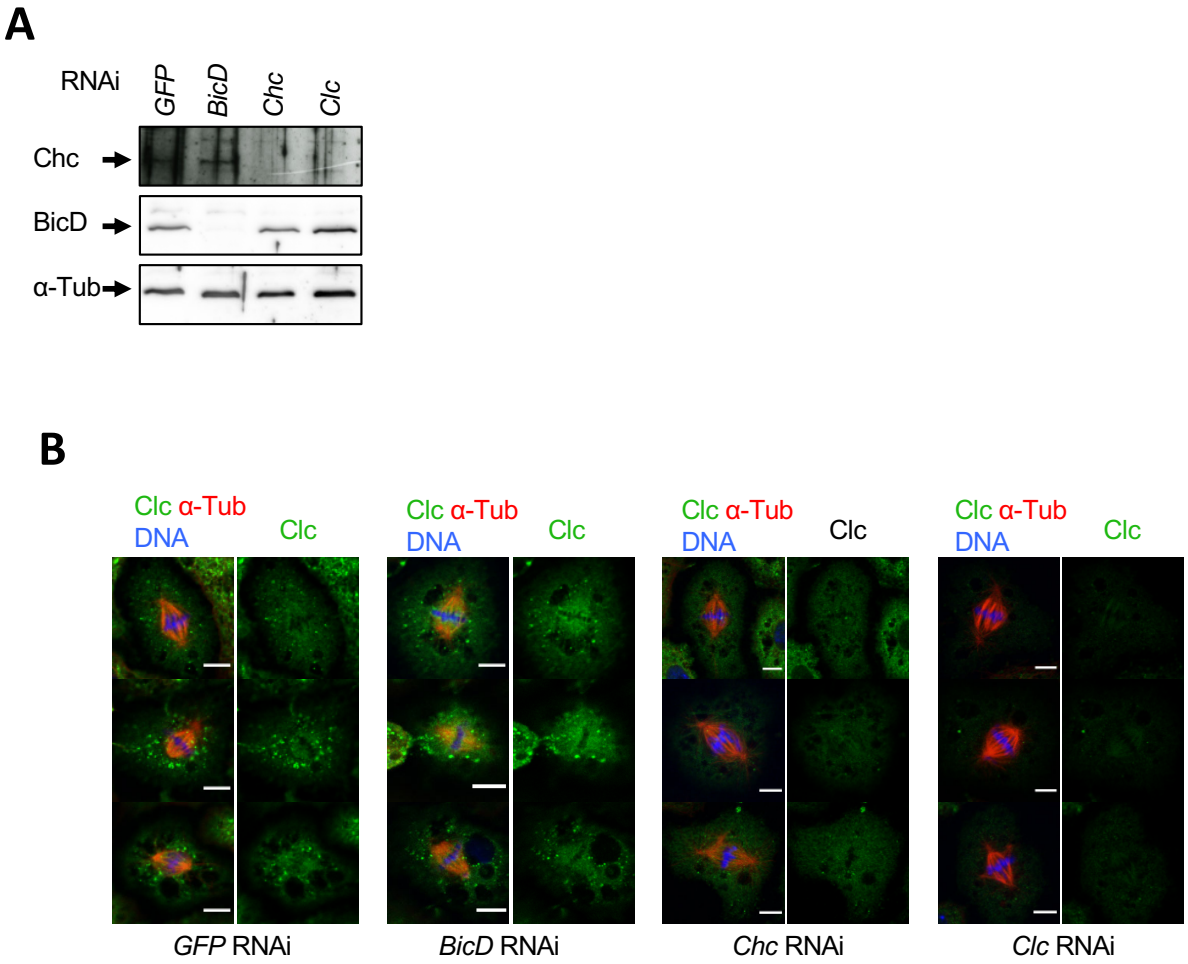

Supplementary Fig. S7